Densification and grain growth during sintering of porous Ce0.9Gd0.1O1.95tape cast layers: A comprehensive study on heuristic methods

Ni, De Wei; Schmidt, Cristine Grings; Teocoli, Francesca; Kaiser, Andreas; Andersen, Kjeld Bøhm; Ramousse, Severine; Esposito, Vincenzo

Published in:
Journal of the European Ceramic Society

Link to article, DOI:
10.1016/j.jeurceramsoc.2013.03.025

Publication date:
2013

Elsevier Editorial System(tm) for Journal of the European Ceramic Society
Manuscript Draft

Manuscript Number: JECS-D-12-01517R1

Title: Densification and grain growth during sintering of porous Ce0.9Gd0.1O1.95 tape cast layers: a comprehensive study on heuristic methods

Article Type: Full Length Article

Keywords: Sintering; Grain growth; CeO2; Porosity; Grain boundary.

Corresponding Author: Dr. De Wei Ni, ph.d.

Corresponding Author's Institution: Technical University of Denmark

First Author: De Wei Ni, ph.d.

Order of Authors: De Wei Ni, ph.d.; Cristine G Schmidt, Ph.D.; Francesca Teocoli, Ph.D.; Andreas Kaiser, Ph.D.; Kjeld B Andersen, Ph.D.; Severine Ramousse, Ph.D.; Vincenzo Esposito, Ph.D.

Abstract: The sintering behavior of porous Ce0.9Gd0.1O1.95 (CGO10) tape cast layers was systematically investigated to establish fundamental kinetic parameters associated to densification and grain growth. Densification and grain growth were characterized by a set of different methods to determine the dominant sintering mechanisms and kinetics, both in isothermal and at constant heating rate (iso-rate) conditions. Densification of porous CGO10 tape is thermally activated with typical activation energy which was estimated around 440-470 kJmol-1. Grain growth showed similar thermal activation energy of 427±22 kJmol-1 in the temperature range of 1100-1250C. Grain-boundary diffusion was identified to be the dominant mechanism in porous CGO10 tapes. Grain growth and densification mechanism were found strictly related in the investigated temperature range. Porosity acts as a grain growth inhibitor and grain boundary mobility in the porous body was estimated around 10-18-10-16 m3N-1s-1 at the investigated temperature range.

DTU Energy Conversion

Frederiksborgvej 399
Building 775
DK-4000 Roskilde
Denmark

March 21, 2013

Dear Editors and Reviewers,

Enclosed please find a revised manuscript: "**Densification and grain growth during sintering of porous $Ce_{0.9}Gd_{0.1}O_{1.95}$ tape cast layers: a comprehensive study on heuristic methods**" by De Wei Ni, Cristine Grings Schmidt, Francesca Teocoli, Andreas Kaiser, Kjeld Bøhm Andersen, Severine Ramousse, and Vincenzo Esposito (Ms. Ref. No.: JECS-D-12-01517).

We thank you for the positive comments and suggestions. We have included the reviewers' suggestions in the enclosed revised version of the manuscript. All the modifications in the manuscript are highlighted in red. Please, find also below the description of the changes, following the order of the comments.

Reviewer #1:

Reviewers' comments:

The present study deals with the densification and grain growth of porous CGO10 during sintering. It is a nice piece of work, since the experiments seems to be correctly conducted and well interpreted.

There is a number of small points which should be addressed before publication:
1) GCO10 and MSC are introduced multiple times in text, while GCO20 none.
2) Page 5, before last line: the freeware software ImageJ - needs citation.
3) Page 10, first line after eq. (4) - there is no reason to indicate the logarithms as exponents.
4) Page 17, eq. (14) and fig. 8 - there is a need of error bar or the confidence degree of the equation, since the lines does not fully fits the points.
5) Caption of fig. 8 - it's not clear
6) Fig. 1 - 'final density' to be replaced with 'final relative density'

Answers:

1) Thanks for the comments. A short description on CGO20 was included in the revised introduction.
2) A reference on freeware software ImageJ was added.
3) The logarithms in page 10, first line after eq. (4) seem superscript (exponent) due to the formulations were inserted into the text as a picture. In the revised version, they were inputted directly into the text and it's all right now.

Technical University of Denmark
DTU Energy Conversion
(Risø campus)

Frederiksborgvej 399
Building 775
DK-4000 Roskilde
Denmark

Tel +45 4677 5778
Fax +45 4677 5858

dwei@dtu.dk
www.ecs.dtu.dk

4) Thanks for your suggestions. Error bars were added in Fig. 8. And correlation coefficients (confidence degree) for all the linear fitting in Fig. 8 are higher than 0.99, which were added in the text.
5) Caption of Fig. 8 was modified in the revised version. It seems clear now.
6) 'Final density' was replaced with 'final relative density' in the description of Fig. 1.

On behalf of the authors,
Best regards,

De Wei Ni
Department of Energy Conversion and Storage, Technical University of Denmark

Densification and grain growth during sintering of porous $Ce_{0.9}Gd_{0.1}O_{1.95}$ tape cast layers: a comprehensive study on heuristic methods

De Wei Ni [*], Cristine Grings Schmidt, Francesca Teocoli, Andreas Kaiser, Kjeld Bøhm Andersen, Severine Ramousse, Vincenzo Esposito

Department of Energy Conversion and Storage, Technical University of Denmark, Frederiksborgvej 399, DK-4000 Roskilde, Denmark.

[*] Corresponding author: dwei@dtu.dk, Tel: +45 4677-5778, Fax: +45 4677-5858

Abstract:

The sintering behavior of porous $Ce_{0.9}Gd_{0.1}O_{1.95}$ (CGO10) tape cast layers was systematically investigated to establish fundamental kinetic parameters associated to densification and grain growth. Densification and grain growth were characterized by a set of different methods to determine the dominant sintering mechanisms and kinetics, both in isothermal and at constant heating rate (iso-rate) conditions. Densification of porous CGO10 tape is thermally activated with typical activation energy which was estimated around 440-470 $kJ \cdot mol^{-1}$. Grain growth showed similar thermal activation energy of ~427±22 $kJ \cdot mol^{-1}$ in the temperature range of 1100-1250 °C. Grain-boundary diffusion was identified to be the dominant mechanism in porous CGO10 tapes. Grain growth and densification mechanism were found strictly related in the investigated temperature range. Porosity acts as a grain growth inhibitor and grain boundary mobility in the porous body was estimated around 10^{-18}-10^{-16} $m^3 \cdot N^{-1} \cdot s^{-1}$ at the investigated temperature range.

Key Words: Sintering; Grain growth; CeO_2; Porosity; Grain boundary.

I. Introduction

Ceria is an important catalytic material that offers high stability, tolerance against harsh environments and electrical conductivity at high temperatures [1, 2]. Particularly, trivalent acceptor doped ceria (*e.g.* A^{3+}, where A is Gd, Sm, Dy *etc.*) has attracted interest for its potential as fast ionic conductor in electrochemical applications [3, 4]. Gadolinium doped ceria (CGO) is the best electrolyte material choice for intermediate temperatures solid oxide fuel cells (IT-SOFC) operating at 600 °C [5-7] and for flue gas purification electrochemical devices [8, 9]. Other applications are as barrier layers in SOFC [10] and oxygen transport membranes operating at high temperatures [11, 12]. Conventionally, the most used doping amounts of gadolinium in ceria are 10mol% and 20mol% (CGO10 and CGO20 for simplification). For most of these applications, CGO is applied as a thin dense layer on a porous support structure. However, highly porous layer allowing gas flow is necessary in catalytic and in gas purification devices. Independent on the final application, tape casting is a very versatile and cost effective large scale production technique [8, 10, 13]. Furthermore, sintering is of great importance for the final microstructure (*e.g.* density and grain size) since it induces most of the morphological transformations at high temperature.

In recent years, numerous models have been proposed for a computer simulation and prediction of sintering behavior. The models are based on constitutive laws of sintering and critically depend on the quality of the experimental input parameters [14-18]. The sintering mechanisms activation energy is a crucial input parameter. This can be derived from the constitutive laws by several methods and characterize densification and grain growth in different conditions such as iso-strain (iso-density) lines approach [17-24] and master sintering curve method (MSC) [25, 26] in iso-rate conditions or Dorn's method in iso-thermal conditions [20, 21, 27, 28]. Both the iso-strain (iso-density) lines approach and MSC method assume that microstructural evolution (both grain size and geometry) are dependent only on density for any given powder and green-body process. Iso-strain (iso-density) lines approach can give out the apparent activation energy evolutions at different densification levels in iso-rate conditions, while

MSC method seeks the best fitting energy value of the entire densification process. MSC is mostly reliable in the case that one diffusion mechanism is dominant in sintering process (*i.e.* constant activation energy) [25]. Conversely to the iso-strain (iso-density) lines approach and MSC method, the Dorn's method gives direct access to the densification activation energy [20, 21, 27, 28] by a series of incremental isothermal heating treatments. These methods have been widely used for CGO, especially for the characterization of dry pressed pellet samples sintering. Several values of activation energy have been reported extensively either for undoped or doped ceria using these methods [19, 24, 29-31]. However, with respect to the tape cast materials, a detailed characterization and investigation on the sintering kinetics and activation energy is still missing. This is probably due to the experimental complications related to the use of slurry-based samples, which present lower density (*i.e.* high porosity) at the green stage. Moreover, supercritical porosity is usually present for green density below 50% [32]. Supercritical porosity is stable in the material during sintering and it can greatly influence densification and grain growth. On the other hand, it has shown that different stress level in the shaping processing can actually influence the particles arrangement in the green body and thus the final densification during sintering [33]. The sintering behavior of low-density tapes is therefore expected to be different from the conventional dry pressing pellets.

In the present work porous CGO10 tape with low-green density relevant for electrolytes in flue gas purification devices, was prepared by tape casting. The densification and grain growth processes of the porous CGO10 tape during sintering were investigated experimentally by optical dilatometry and microscopy. Based on the achieved results, the activation energies for densification and grain growth were evaluated and compared using different approaches (iso-density lines approach, master sintering curve (MSC) method, as well as Dorn's method), which provided insight into the densification mechanisms. For comparison, the sintering behavior of CGO10 dry pressing pellet was also studied. More generally, this investigation provided a fundamental understanding for densification and grain growth activation energy evaluation by different methods in terms of porous tape cast layer.

II. Experimental procedures

2.1 Material and tape casting

$Ce_{0.9}Gd_{0.1}O_{1.95}$ with low surface area (12.8 m^2/g, Rhodia S.A., France) was used as starting materials. Two graphite pore formers (V-UF1 99.9, d_{50}: 2.6μm, Graphit Kropfmühl, Germany and SGB 10 L/99.9, d_{50}: 10μm, Graphit Kropfmühl, Germany) were used in order to obtain sufficient open porosity and pores with suitable shape and size (mainly in respect to use in flue gas purification devices), so that the pores could connect to each other very well. The amounts of the two graphite pore formers were ~4.8 wt% and 2.1wt%, respectively. The resulting powder mixture was dispersed in a methylehylketone and ethanol (MEKET) based suspension with polyvinyl-pyrrolidone (PVP) as dispersant and polyvinylbutyral (PVB) as binder [34]. The resulting slurry for tape casting was homogenized by ball milling for 72 hours. It was tape-casted on Mylar® foil at constant speed (20 cm/min) in a controlled environment with a blade clearance around 150 μm. The final thickness of the CGO10 tape was approximately 30 μm (green tapes after drying). The CGO green tape was tight rolled and pressed to obtain "bulky" sample of the thin layer which allowed dilatometry measurement. Final shapes of the samples were obtained by cutting the rolled tapes in cylindrical chips of about 5-8 mm in length and 3-5 mm in diameter.

2.2 Dilatometric measurement

Dilatometric measurements were performed by an optical dilatometer (TOMMI, Fraunhofer ISC, Würzburg, Germany). This allows following samples shape evolution during sintering by *in-situ* and non-contact, simply collecting the sequent images of the samples' silhouettes projected by a source of visible light onto a high definition camera [17, 23]. "Non-contact" measurement is critical for the tape casting layer due to its intrinsic poor mechanical properties before sintering. The complete thermal cycle including de-binding, pore former removal and sintering, was performed directly in the optical

dilatometer to avoid any possible stress on the samples. The de-binding cycle included a slow heating ramp at 0.33 °C/min step from room temperature to 400 °C, and an isothermal treatment step at 400 °C for 4h to ensure the binders removal. After binder burnout, the samples were fired at the same heating rate to 800°C and held for 2h to remove the graphite pore former. The samples were then heated to 1250 °C (after 800 °C) at heating rates of 0.33, 1 and 5 °C/min. Different heating rates were performed for the iso-density lines approach and the MSC method study. For the Dorn's method, the temperature increment was given at a step of 15 °C/min in a temperature range of 900-1080 °C in a sequence of 6 steps, with holding of 20 minutes at each step.

The linear strain (ε) was monitored *in situ* continuously during the heating and cooling cycles. Thermal expansion of the samples was corrected using the thermal expansion coefficient (TEC) determined from the cooling part of the shrinkage curve. The relative densities (ρ) as a function of temperature is calculated from the linear strain data assuming an isotropic shrinkage behavior:

$$\rho(T) = \rho_0 \exp(-3\varepsilon) \tag{1}$$

where ρ_0 is the relative density of green sample.

2.3 Microstructure and grain growth

To study the grain growth behaviour of the as-prepared CGO10 tape, the green samples were sintered at four different sintering temperatures with different holding time. Cross sections of the sintered samples were polished and thermally etched at temperatures 100 °C lower than their respective sintering temperatures for 0.5 h to reveal grain boundaries. And microstructures were observed using field emission scanning electron microscopy (FE-SEM, Supra, Carl Zeiss, Germany). The porosity and grain size after sintering were determined by post processing of the SEM images, using freeware software ImageJ® [35]. To reduce the error in the determination of porosity, at least ten images with hundreds of pores were taken

in random regions of the samples and used for the statistical analysis. The relative density was estimated as deduction of porosity. Average grain sizes of the sintered materials were determined by linear intercept method from at least 100 randomly selected grains.

III. Results and discussion

3.1 Comparison of sintering behavior between CGO10 dry pressing pellet and tape cast layer

To clarify the difference in the densification behavior between CGO10 dry pressing pellet and porous tape cast layer, the shrinkage of these two kinds of samples (prepared using identical starting powders) during sintering was studied and compared at first. **Fig. 1** shows the variations of shrinkage with temperature at a heating rate of 1°C/min in the temperature range of 800-1250 °C, the inset is the linear strain rate of the two samples. The strain curve of the CGO10 tape cast layer shows similar trend to that of the dry pressing pellet. However, CGO10 tape shows slower shrinkage behavior compared with the dry pressing pellet at lower temperature, whereas it becomes faster as temperature increases. Simultaneously, it can also be found that the temperature at which the CGO10 tape starts to shrink is a little higher compared to the dry pressing pellet. Their difference is shown more clearly in the strain rate plots inserted in **Fig. 1**. The CGO10 dry pressing pellet shows a higher strain rate at the temperature lower than ~950 °C, and achieves its highest shrinkage rate at about 1080 °C. Whereas the CGO10 tape has a faster strain rate in the temperature range of 950-1250 °C and achieves its highest shrinkage rate at about 1060 °C. This indicates that the densification of CGO10 tape is significantly enhanced compared with the dry pressing pellet at higher temperatures. The repeat of the dilatometric measurement shows good reproducibility for the tape cast samples. Pressed pellets samples can present different sintering behavior depending on the shaping techniques [33]. Therefore, it can be rest assured that the sintering behavior

difference between CGO10 pellet and tape is resulted from their intrinsic microstructural characteristics at the green stage.

Green density, particles and pores arrangement in green samples are important factors influencing mass diffusion during sintering. In this study, the green density of the CGO10 dry pressing pellet was estimated about 0.55 from the geometric shape after cold isostatic pressing. The relative density was about 0.40 for the CGO10 tape after de-binding and pore former removal. Green density for tapes was estimated by the dilatometry data considering the rolled sample isotropic and counting that the measured final relative density of the sample was at 0.63. As expected, the CGO10 dry pressing pellets exhibited a relatively lower onset temperature for densification, and showed a faster shrinkage rate at lower temperature. Normally, colloid processing (*e.g.* tape casting and slip casting) can obtain uniform microstructure with uniform particle arrangement and less agglomeration, compared to conventional powder processing (*e.g.* dry pressing). This can lead to faster shrinkage and higher densification. In another work, some of the authors of this paper have shown that different stress level in the shaping processing can actually influence the particles arrangement in the green body and thus the final densification during sintering. Particularly, it was demonstrated that high packing at the green stage cannot result in the higher final density in the case that the sintering shaping stress is high [33]. According to this result, it is confirmed that accurate analysis of the sintering kinetics of tape cast layer cannot be carried out on pressed pellet samples and original shaped samples must be investigated.

3.2 Determination of densification kinetics of CGO10 tape

3.2.1 TOMMI measurement of CGO10 tape during sintering at different heating rates

The strains during sintering of porous CGO10 tape cast layer were measured *in-situ* and non-contact using a thermo-optical measuring technique (optical dilatometer, TOMMI). The non-contact techniques allow following densification process during firing for samples of diverse shapes in a large

range of shape evolutions. The optical system in TOMMI is designed to project the sample shadow silhouette into a high resolution camera [17, 23]. This can register both swelling and shrinkage in a range of sizes and directions that conventional contact dilatometer cannot register. Optical dilatometry is particularly reliable for the characterization of tape-cast and slurry based samples, where high amount of organic component can lead to drastic change in the sample shape during the firing process [33, 36].

Based on the shrinkage strains *in situ* measured by TOMMI, the relative densities of porous CGO10 tapes sintered at different heating rates were calculated using Eq. (1). **Fig. 2** shows the variations of relative density with sintering temperature at different heating rates in the temperature range of 800-1250 °C. It can be seen that the relative density in **Fig. 2** increased continuously with the sintering temperature in the investigated sintering temperature range (800-1250 °C). The porous CGO10 tape starts to densify at about 850 °C and the onset temperature slightly increases as heating rate increases. Remarkable densification is observed at temperatures above 900 °C. The densification proceeds without the typical plateau of the final stage of the sintering, indicating that the residual porosity is not stable and it can be further reduced by firing at high temperatures. The porous CGO10 tape studied in this work was designed for flue gas purification. Therefore a large amount of graphite pore-former was added. After de-binding and pore-former removal, typical porous CGO10 tape reaches relative density of 0.40 (*i.e.* white density). The final relative density at 1250 °C at the heating rate of 0.33 °C/min is about 0.664. The sintering profile changed at different heating rates leading to final density of 0.626 and 0.607 at the heating rates of 1 and 5 °C/min, respectively. Porosity values of around 35% would fulfill the requirements of free passage of the gases through the flue gas purification devices, assuming that the most of the porosity is open and connected [8, 9]. According to results in **Fig. 2**, such a density locates at the early stage sintering for the investigated temperatures range [18].

The densification rates of the porous CGO10 tape during sintering were also evaluated from the time derivatives of the density curves (inset **Fig. 2**). Densification rate curves conveniently display samples sintering activity at different heating conditions. Particularly, the inset plots in **Fig. 2** show that

the densification rate increases with the sintering temperature, attaining a peak of activity and then decreasing with the temperature. Furthermore, as the heating rate increases, the maximum densification rate increases and shifts towards higher temperatures. The densification rates peaks are achieved at about 1010, 1060 and 1090 °C respectively as heating rate increases. These results are also consistent with those reported by He *et al* [19] on CGO10 pellets densification behavior.

3.2.2 Densification kinetics analysis based on constitutive laws

Shrinkage during sintering is driven by thermally activated forces generated in the porous compacts by interface energy minimization between particles, pores, and grains. Surface diffusion, grain boundary diffusion and volume diffusion are the three main thermally activated mechanisms for mass transfer, which can occur simultaneously during sintering [37]. In the constitutive laws for densification, the densification rate is expressed as a function of activation energy (Q), which includes all the mechanisms generated during sintering [16, 17]. The strain rate is usually described by the formula:

$$-\frac{d\varepsilon}{dt}=\frac{1}{3\rho}\frac{d\rho}{dt}=\frac{C_1(\rho)\gamma D}{kTG^n}=\frac{C_1(\rho)\gamma D_0}{kTG^n}\exp(-\frac{Q}{RT}) \tag{2}$$

where ε is the true strain, ρ is relative density, t is time, C_1 is a constant depending on microstructure, γ is the solid-gas interface energy, D is the diffusion coefficient, Q is the apparent activation energy for diffusion mechanism leading to densification, R is the gas constant, k is Boltzmann constant, T is absolute temperature, G is mean grain size, n is a parameter depending on mechanism (3 for volume diffusion and 4 for grain boundary diffusion). According to the Eq. (2) the densification is thus function of density (porosity) and of some simplified microstructural constants (C_1, n) and grain size (G). However, grain size and porosity change with temperature and individual mechanisms cannot be identified by this approach. Nevertheless, such assumptions are convenient for the estimation of the activation energy of the

whole process, especially when sintering is strongly affected by a dominant mechanism. This is the case of doped ceria which is known to be limited by dominant grain boundary solute drag diffusion [29, 30].

(1) iso-strain (iso-density) lines approach

Rearranging and taking the logarithm of both sides of Eq. (2), the following equations can be obtained:

$$\ln(-T\frac{d\varepsilon}{dt}) = -\frac{Q}{R}\frac{1}{T} + \ln(\frac{C_1(\rho)\gamma D_0}{k}) - n\ln G \tag{3}$$

$$\ln(T\frac{d\rho}{dt}) = -\frac{Q}{R}\frac{1}{T} + \ln(\frac{3\rho C_1(\rho)\gamma D_0}{k}) - n\ln G \tag{4}$$

Logarithmic curves of $ln(-T\frac{d\varepsilon}{dt})$ or $ln(T\frac{d\rho}{dt})$ as a function of the reciprocal absolute temperature (*1/T*) measured during sintering of green compacts with different constant heating rates can be plotted according Eqs. (3) or (4). Then, points of equal strain (density) on different shrinkage curves can be connected to form so-called iso-strain (iso-density) lines. With the same densification level, the grain sizes are usually identical. Especially in the present work, the effect of grain growth is very limited in the studied density range (ρ<0.7). Therefore, straight lines could be obtained for the iso-strain (iso-density) lines respectively. From the slopes, the activation energy *Q* for densification can be calculated for the respective iso-strain (iso-density) conditions [17, 19-23].

Fig. 3 shows the corresponding plots for the evaluation of activation energy for densification of porous CGO10 tape based on the iso-density lines approach. As expected, the evaluation with the model described above leads to straight iso-density lines for all the investigated density values. Correlation coefficients for all the linear fitting in **Fig. 3** are higher than 0.98. Moreover, all the fitted lines are almost parallel to each other, indicating an independency of the activation energy on the relative density in the analyzed densification regime. The activation energy for densification in the investigated density range

(0.46-0.60) is evaluated to be 470±31 kJ·mol^{-1}. Chen [30] reported that the activation energy for densification of pure ceria and 1% gadolinium oxide doped ceria pellets in air is 6.16 eV (~593 kJ·mol^{-1}) and 4.66 eV (~449 kJ·mol^{-1}) respectively, and Jud *et al* [24] reported that the activation energy for densification of CGO20 pellet is 4.70±0.32 eV (~453±31 kJ·mol^{-1}) in the relative density range of 0.65-0.90. Therefore, the determined activation energy for densification of porous CGO10 tape, at the early-stage of the sintering, is comparable to those reported for dry pressing pellets in literature.

The estimation of grain size evolution with the temperature for the calculation of the densification activation energy in Eq. (2) can be theoretically distinguished from the densification mechanisms by evaluating the grain growth exponent *n*. Rearranging and taking the logarithm on both sides of Eq. (2), and including grain growth during sintering, a new formula gives the necessary equation for the determination of the activation energy:

$$\ln(TG^n \frac{d\rho}{dt}) = -\frac{Q}{R}\frac{1}{T} + \ln(\frac{3\rho C_1(\rho)\gamma D_0}{k}) \tag{5}$$

However, fits with low errors can be obtained for both *n* equals to 3 (volume diffusion) and 4 (grain boundary diffusion). And the activation energy exhibits in the case *n*=3 (~436±31 kJ·mol^{-1}) slightly lower value than the one for *n*=4 (~461±26 kJ·mol^{-1}). Volume diffusion normally exhibits higher activation energy than grain boundary diffusion, but diffusion in the case of solute drag mechanism at grain boundary can result highly energetic [30]. However, the adopted method does not allow distinguishing the densification mechanisms. This limitation has also been reported for sintering models based on the constitutive law for other systems [24, 30]. Other limitations are the relatively poor resolution of the applied plotting method, the constitutive scattering of dilatometric data, and the limiting assumption that C_1 is a constant with the temperature.

(2) Master sintering curve (MSC)

Master sintering curve (MSC) is another simple yet powerful approach to describe the sintering process [25, 26]. The concept of a MSC is based on the premise that the density of a sintering body is a unique function of its thermal history (*i.e.* all thermal histories can be reduced to a common relationship with relative density). Eq. (2) can be rearranged and integrated as follows:

$$\frac{k}{\gamma D_0}\int_{\rho_0}^{\rho}\frac{G^n}{3\rho C_1(\rho)}d\rho=\int_0^t\frac{1}{T}\exp(-\frac{Q}{RT})dt \tag{6}$$

$$\Phi(\rho)\equiv\frac{k}{\gamma D_0}\int_{\rho_0}^{\rho}\frac{G^n}{3\rho C_1(\rho)}d\rho \tag{7}$$

$$\Theta(t,T(t))\equiv\int_0^t\frac{1}{T}\exp(-\frac{Q}{RT})dt \tag{8}$$

In such a simplification, it can be found that the $\Phi(\rho)$ is a microstructure-related function, whereas $\Theta(t, T(t))$ depends only on Q and the time-temperature profile. Differently from the iso-density method, no microstructural parameters directly appear in the equations in MSC. The constants used in Eq. (2) are thus "reduced" to a general microstructural function, which includes all the possible microstructural evolutions as effect of the densification during sintering. By the MSC method, the relationship between the relative density ρ and $\Theta(t, T(t))$ is defined and possible solutions of the Eq. (8) are considered to estimate the activation energy of the dominant phenomena. The value of activation energy that yields the minimum mean residual square (MRS) is thus selected for the construction of MSC. Subsequent iterations allow for the calculation of densification curves for arbitrary time-temperature cycles. Vice versa, the time-temperature cycle can be calculated which provides prescribed densification rates.

In order to plot the master sintering curve, relative density ρ obtained at different heating rates is plotted against $\Theta(t, T(t))$ and the value of Q is adjusted where data fall on a single curve. The best fit is determined by minimizing the MRS deviation function:

$$\Delta(\ln(\Theta)) = \int_{\rho_0}^{\rho_f} \frac{(\sum_{i=1}^{N}(\ln(\Theta_i) - \ln(\Theta_{av}))^2)^{\frac{1}{2}}}{N(\rho_0 - \rho_f)} d\rho \quad (9)$$

where the summation is over the different heating rates, ρ_0 and ρ_f are the green and final densities. **Fig. 4** shows the MSC of porous CGO10 tape and inset shows MRS deviation function plotted against Q with minimum value of the best fit at 440±20 kJ·mol^{-1}. This activation energy value is in good agreement with the results from the iso-density lines method shown in **Fig. 3**. Using this value of Q= 440 kJ·mol^{-1}, the MSC for sintering of porous CGO10 tape was constructed, as shown in **Fig. 4**. It can be found that an excellent fitting was established based on the three densification curves in **Fig. 2**. The satisfactory construction of MSC reveals that the assumption for MSC establishment is satisfied in the present work. Limitations in using MSC approach are usually registered where sintering is a well-defined sequence of different mechanisms. In such cases the MSC can result difficult at the different level of densification [25]. Therefore, the microstructural evolution (both grain size and geometry) in porous CGO10 tape-cast sample are dependent mainly on density for the given powder and green body process, and most likely one dominant diffusion mechanism is occurring in the sintering process.

(3) Dorn's method

Conversely to the other methods, the Dorn's method gives direct access to the densification activation energy [20, 21, 27, 28] by a series of incremental isothermal heating treatments. Such an approach is commonly used to measure the activation energy of creep phenomena, and it thus can also be used to study sintering. By the Dorn's method, the isothermal strain rate is recorded firstly at a temperature T_1 for a sintering time t, then, following a temperature increment made as rapid as possible, the same recording is made at a temperature T_2, slightly higher than T_1. In such conditions, it can be assumed that the microstructural state remains unchanged during the temperature increment, and then the following equality can be obtained:

$$(\varepsilon)_{end\ step\ T_1} = (\varepsilon)_{beginning\ step\ T_2} \tag{10}$$

From Eq. (2), the ratio between the corresponding strain rates $\dot{\varepsilon} = \frac{d\varepsilon}{dt}$ can be expressed as:

$$\frac{\dot{\varepsilon}_2}{\dot{\varepsilon}_1} = \frac{T_1}{T_2} \exp\left(\frac{-Q}{R} (\frac{1}{T_2} - \frac{1}{T_1}) \right) \tag{11}$$

The densification activation energy is then deduced from:

$$Q = \frac{RT_1T_2}{T_2 - T_1} \ln\left(\frac{T_2\dot{\varepsilon}_2}{T_1\dot{\varepsilon}_1} \right) \tag{12}$$

An important assumption is that the microstructural state remains unchanged during the temperature increment. However, this may not always be the case during isothermal experiments especially at high densification levels. As well, isothermal holding may influence the sintering behavior at subsequent sintering steps as sintering proceeds. It is hence important that a short isothermal holding is used to reduce its influence on the subsequent sintering steps, while it must still be long enough to achieve thermal equilibrium at every isothermal step. The method better suits the early stage of sintering and an appropriate temperature interval is recommended to reduce the possible microstructural change during the temperature increment. For the porous CGO10 samples, the temperature increment was given at a step of 15 °C/min and an interval 30 °C from 900 °C to 1080 °C, and a holding of 20 minutes at each step was used. **Fig. 5** shows the determined activation energy for densification of porous CGO10 tape for each temperature step using Dorn's method. It was evaluated to be 453±27 kJ·mol^{-1}. This is again in good agreement with the results from the iso-density lines and MSC methods.

Comparing the results obtained from different methods, some simple considerations can be done. The three methods are based on the characterization of densification, as a function of the linear strain, by dilatometry. As a consequence, the accuracy of the data acquisition is crucial especially for those samples, as slurry-based ones, which can present drastic shape evolution during firing. In the iso-rate conditions,

the MSC gives a "best-fitting" energy value of the overall thermally activated phenomena while the iso-density lines approach gives out a series of activation energy at respective densification levels. Such values in the porous CGO tape samples, at the investigated density range (0.47-0.60), resulted almost constant. The Dorn's method also gives as result the values of activation energy at each thermal step. However, these resulted slightly different at the different steps, ranging from 417 to 479 kJ/mol. Particularly, **Fig. 5** shows that CGO10 tapes present a peak of thermal activation energy at temperatures between 950 and 1050 °C. Such a result is consistent with data in **Fig. 2** which shows a critical activity of sintering activity as function of the temperature. Although, the variation of the determined activation energy in the studied densification range is limited, the Dorn's method seems to represent in a better detail the thermal diffusivity in the sample than a representation limited to the level of densification. This can be explained by the fact that diffusive phenomena are better described by the thermal energy level than on the microstructure, especially when this is evolving in a narrow range of density and porosity variations.

Despite such differences, results showed that various heating cycles for the studied porous CGO10 tape can be described by the same MSC using constant thermal activation energy. It is proved that all the values of activation energy calculated by the three different methods match with each other quite well, no matter whether taken in iso-rate or iso-thermal conditions. This indicates that the assumptions for these methods, such as microstructure evolution during sintering only dependent on density, microstructural state unchanged during temperature increment in Dorn's method, *etc*. are basically correct in the present study. It also indicates that the whole investigated sintering process was dominated by a same diffusion mechanism. Such individual mechanism, however, cannot be distinguished by dilatometry and a direct microstructural characterization is needed.

3.3 Determination of grain growth kinetics of CGO10 tape

The above methods give out the apparent densification activation energy only based on the geometry (*i.e.* strain or density) evolution during sintering, which do not refer to any particular microstructures. However, the driving force in sintering is related to the microstructural features because it depends mainly on the surface energy at the grain boundaries and pore/grain interface. The grain growth of porous CGO10 tape during early stage sintering was also investigated to clarify the relation between microstructure and densification in the sintering kinetics. As an illustration, high resolution SEM images of CGO10 tape sintered at 1250 °C/0h and 1250 °C/4h are shown in **Fig. 6**.

The average grain size, *G*, was evaluated from the SEM images and **Fig. 7** displays the variations of grain size versus isothermal time at different temperatures. This shows that the grain size increases with sintering proceeds for all the investigated CGO10 tapes at different heating temperatures. Grain growth is very slow for the CGO10 samples sintered at 1100-1200 °C, which becomes faster for the samples sintered at 1250 °C. This is expected in CGO because the high dopant level constrains the growth by solute drag effect especially at low temperatures [30]. However, compared to the dry pressing pellets, the grain growth in the investigated porous CGO10 tape in the initial stage of sintering is very limited overall [19, 31], indicating a certain inhibition of the sintering process due to the large porosity in the samples. The latter is expected especially where supercritical porosity (stable) is present in the material [32, 37]. Although in CGO porous tapes final stage of the sintering was not achieved, both dilatometry (see, **Fig. 1**) and microscopy analysis (not shown here) suggested that supercritical porosity induced by use of graphite pore-former was pretty high at around 20-30 % of the total volume.

Normally, grain growth kinetics is analyzed under isothermal conditions from grain size vs. time curves (**Fig. 7**), in accordance with the well-known grain growth kinetics equation: [31, 38]

$$G_t^{\,m} - G_0^{\,m} = Kt = K_0 t \exp(-\frac{Q_g}{RT}) \tag{13}$$

where G_t is the average grain size at time t, G_0 is the initial grain size, m is the kinetic grain growth exponent typically between 2 and 4, K is a rate constant, K_0 is a pre-exponential constant, Q_g is the

apparent activation energy for grain growth, R is the gas constant and T is the absolute temperature. The kinetic grain growth exponent m for CGO was assumed to be 2 from Chen *et al* [30]. And therefore Eq. (13) can also be rewritten as:

$$Ln(G_t^2 - G_0^2) = LnK_0 + Lnt - \frac{Q_g}{RT} \tag{14}$$

Fig. 8 shows the corresponding plots for the evaluation of activation energy for grain growth based on Eq. (14). It is shown that data are well fitted in by linear functions fitting and the activation energy for grain growth of CGO10 tape was evaluated by the slope to be 427±22 kJ·mol^{-1}. Correlation coefficients for all the linear fitting in **Fig. 8** are higher than 0.99. The pre-exponential constant K_0 was also calculated, with a value of 0.04 m^2·s^{-1}, which represents the grain growth rate to some extent. The fitting of grain growth exponent m equals to 3 and 4 was also conducted in this work, but the linear regression was unacceptable. This suggests that the assumption of m=2 is reasonable and grain growth of the porous CGO10 tape proceeds predominantly through grain boundary diffusion mechanism [30, 31]. It is also found that the evaluated activation energy for grain growth is very close to that determined for densification of CGO10 tape. Therefore, we can conclude that the densification processes of porous CGO10 tape in the early stage of sintering are dominated by the same diffusion mechanism.

Grain growth kinetics Eq. (13) can also be rewritten as [29, 30]:

$$G_t^2 - G_0^2 = 2M\gamma(t - t_0) \tag{15}$$

where M is the grain boundary mobility, γ is grain boundary energy. From the grain growth kinetics analyzed above, grain boundary mobility can be evaluated. In the analysis of the sintering processes, the grain boundary energy of the material is generally taken constant. For doped-ceria systems grain boundary energy is $\gamma \approx 0.3$ J·m^{-2} [29]. The grain boundary mobility for the porous CGO10 tape was calculated about 10^{-18}-10^{-16} m^3·N^{-1}·s^{-1} in the investigated temperature range (1100-1250 °C), which is estimated to be around 1-2 order of magnitude smaller than the corresponding dry pressing pellet [29].

This confirms that porosity acts as grain growth inhibitor during sintering. The forces driving the sintering are generated by energy minimization processes at the surface of particles and grains. Such phenomena are carried out via mass diffusion mechanisms and lead to spontaneous contacting, adhesion, densification and growth of the particles. High porosity can decrease the chance of particle contact, and grain boundary mobility is therefore slowed, which leads to the slower grain growth for the investigated porous CGO10 tape.

Similarly to the MSC, we can also define:

$$\Theta_g \equiv K_0 t \exp(-\frac{Q_g}{RT}) \tag{16}$$

Therefore, Eq. (13) can be rewritten as:

$$G_t^{\,2} - G_0^{\,2} = \Theta_g \tag{17}$$

The relationship between G_t and Θ_g can be regarded as a grain growth master curve [39]. Based on the evaluated pre-exponential constant K_0 and activation energy Q_g for grain growth, the grain growth master curve for sintering of porous CGO10 tape was constructed, as shown in **Fig. 9**. Our experimental measurements for CGO10 tape sintered at different temperatures and times are also shown in **Fig. 9**, well fitted to the constructed grain growth master curve.

V. Conclusion

Compared to dry pressing pellet, the porous CGO10 tapes showed different densification behavior due to their different green density and particle arrangement. This work investigated the densification and grain growth kinetics in the early-stage sintering of porous CGO10 tape. The sintering kinetics and activation energy for densification were determined employing three different methods: iso-density lines approach, master sintering curve (MSC), and the Dorn's method. The iso-density lines

approach and Dorn's method gave out a series of activation energy at respective densification levels, whereas the variation of the determined values in the investigated densification range is very limited. For the MSC method, constant activation energy was determined for the entire sintering process. All the three methods produced similar kinetics results with densification activation energy of around 440-470 $kJ \cdot mol^{-1}$. This indicated that the whole investigated sintering process is dominated by a unique diffusion mechanism. Moreover, the activation energy for grain growth was evaluated to be ~427±22 $kJ \cdot mol^{-1}$ in the temperature range 1100-1250 °C and the grain growth master curve was constructed. It is indicated that both the densification and grain growth processes for porous CGO10 tape are dominated by grain boundary diffusion mechanism. The determined activation energy for densification energy and grain growth of porous CGO10 tape is comparable to those values reported for gadolinium oxide doped ceria dry pressing pellets in literature. However, due to the high porosity, the grain boundary mobility for porous CGO10 tape (10^{-18}-10^{-16} $m^3 \cdot N^{-1} \cdot s^{-1}$) was estimated around 1-2 order of magnitude smaller than the corresponding dry pressing pellet in the investigated temperature range, which led to the slower grain growth behaviour in porous CGO10 tape.

Acknowledgement:

The authors would like to acknowledge the support of the Scientific Research Councils on Technology and Production Sciences (FTP) (Contract No. 09-072888, OPTIMAC), which is part of the Danish Council for Independent Research (DFF). Discussions with Karsten Agersted and Nini Pryds from DTU Energy Conversion and Storage Department are highly appreciated.

References:

[1] Mogensen, M., Sammes, N. M. and Tompsett, G. A., Physical, chemical and electro-chemical properties of pure and doped ceria. *Solid State Ionics*, 2000, **129**, 63-94.

[2] Kleinlogel, C. and Gauckler, L. J., Sintering and properties of nanosized ceria solid solutions. *Solid State Ionics*, 2000, **135**, 567-573.

[3] Wang, S., Kobayashi, T., Dokiya, M. and Hashimoto, T., Electrical and ionic conductivity of Gd-doped ceria. *J. Electrochem. Soc*., 2000, **147**, 3606-3609.

[4] Gorte, R. J., Kim, H. and Vohs, J. M., Novel SOFC anodes for the direct electrochemical oxidation of hydrocarbon. *J. Power Sources***,** 2001, **106**, 10-15.

[5] Meier, L. P., Urech, L. and Gauckler, L. J., Tape casting of nanocrystalline ceria gadolinia powder. *J. Eur. Ceram. Soc.*, 2004, **24**, 3753-3758.

[6] Cheng, J., Zha, S., Fang, X., Liu, X. and Meng, G., On the green density, sintering behavior and electrical property of tape cast $Ce_{0.9}Gd_{0.1}O_{1.95}$ electrolyte films. *Mater. Res. Bull*., 2002, **37**, 2437-2446.

[7] Atkinson, A. and Selcuk, A., Mechanical behaviour of ceramic oxygen ionconducting membranes. *Solid State Ionics*, 2000, **134**, 59-66.

[8] Christensen, H. and Rak, Z. S., A novel diesel particulate converter. *Catal. Today*, 2002, **75**, 451-457.

[9] He, Z., Andersen, K. B., Keel, L., Nygaard, F. B., Menon, M. and Hansen, K. K., Processing and characterization of porous electrochemical cells for flue gas purification. *Ionics*, 2009 **15**, 427-431.

[10] Simner, S. P., Anderson, M. D., Engelhard, M. H. and Stevenson, J.W., Degradation mechanisms of La-Sr-Co-Fe-O_3 SOFC cathodes. *Electrochem. Solid State Lett.*, 2006, **9**, A478-481.

[11] Steele, B. C. H., Oxygen-transport and exchange in oxide ceramics, *J. Power Sources*, 1994, **49**, 1-14.

[12] Ji, Y., Kilner, J. A. and Carolan, M. F., Electrical conductivity and oxygen transfer in gadolinia-doped ceria (CGO)-$Co_3O_{4-\delta}$ composites. *J. Eur. Ceram. Soc.*, 2004, **24**, 3613-3616.

[13] Klemensø, T., Menon, M. and Ramousse, S., Low toxicity binder systems for tape cast $Ce_{0.9}Gd_{0.1}O_{1.95}$ laminates. *Ceram. Int.*, 2010, **36**, 773-780.

[14] Riedel, H., Zipse, H. and Svoboda, J., Equilibrium pore surfaces, sintering stresses and constitutive equations for the intermediate and late stages of sintering. II. Diffusional densification and creep. *Acta Metall. Mater.*, 1994, **42**, 445-452.

[15] Camacho-Montes, H., Garcia-Casillas, P. E., Rodriguez-Ramos, R., Fuentes-Montero, M. E. and Fuentes-Cobas, L. E., Simulation of the stress-assisted densification behavior of powder compact: effect of constitutive law. *J. Am. Ceram. Soc.*, 2008, **91**, 836-845.

[16] Rahaman, M. N., *Sintering of Ceramics*, CRC Press, Boca Raton, 2008.

[17] Raether, F. and Horn, P. S., Investigation of sintering mechanisms of alumina using kinetic field and master sintering diagrams. *J. Eur. Ceram. Soc*., 2009, **29**, 2225-2234.

[18] He, Z. M. and Ma, J., Constitutive modeling of the densification of micron-grain-sized alumina ceramics. *Philos. Mag.*, 2003, **83**, 1889-1916.

[19] He, Z. M., Yuan, H., Glasscock, J. A., Chatzichristodoulou, C., Phair, J. W., Kaiser, A. and Ramousse, S., Densification and grain growth during early-stage sintering of $Ce_{0.9}Gd_{0.1}O_{1.95-\delta}$ in a reducing atmosphere. *Acta. Mater*., 2010, **58**, 3860-3866.

[20] Dehaudt, P., Bourgeois, L. and Chevrel, H., Activation energy of UO_2 and UO_{2+x} sintering. *J. Nucl. Mater.*, 2001, **299**, 250-259.

[21] Lahiri, D., Ramana Rao, S. V., Hemantha Rao, G. V. S. and Srivastava, R. K., Study on sintering kinetics and activation energy of UO_2 pellets using three different methods. *J. Nucl. Mater.*, 2006, **357**, 88-96.

[22] Wang, J. and Raj, R., Estimate of the activation energies for boundary diffusion from rate-controlled sintering of pure alumina, and alumina doped with zirconia or titania. *J. Am. Ceram. Soc.*, 1990, **73**, 1172-1175.

[23] Raether, F., Current state of in-situ measuring methods for the control of firing processes. *J. Am. Ceram. Soc.*, 2009, **92**, S146-152.

[24] Jud, E., Huwiler, C. B. and Gauckler, L. J., Sintering analysis of undoped and cobalt oxide doped ceria solid solutions. *J. Am. Ceram. Soc.*, 2005, **88**, 3013-3019.

[25] Su, H. H. and Johnson, D. L., Master sintering curve: a practical approach to sintering. *J. Am. Ceram. Soc.*, 1996, **79**, 3211-3217.

[26] Hansen, J. D., Rusin, R. P., Teng, M. H. and Johnson, D. L., Combined-stage sintering model. *J. Am. Ceram. Soc.*, 1992, **75,** 1129-1135.

[27] Dorn, J. E., pp. 255-83 in Creep and Recovery. Edited by R. Maddin. American Society for Metals, Cleveland, Ohio, 1957.

[28] Bacmann, J. J. and Cizeron, G., Dorn method in the study of initial phase of uranium dioxide sintering. *J. Am. Ceram. Soc*., 1968, **51**, 209-212.

[29] Chen, P. L. and Chen, I. W., Role of defect interaction in boundary mobility and cation diffusivity of CeO_2. *J. Am. Ceram. Soc.*, 1994, **77**, 2289-2297.

[30] Chen, I. W., Grain boundary kinetics in oxide ceramics with the cubic fluorite crystal structure and its derivatives. *Interf. Sci.*, 2000, **8**, 147-156.

[31] Li, J. G., Ikegami, T. and Mori, T., Low temperature processing of dense samarium-doped CeO_2 ceramics: sintering and grain growth behaviors. *Acta. Mater*., 2010, **52**, 2221-2226.

[32] Chen, P. L. and Chen, I. W., Sinering of fine oxide powders: I, microstructural evolution. *J. Am. Ceram. Soc.*, 1996, **79**, 3129-3141.

[33] Glasscock, J. A., Esposito, V., Foghmoes, S. P. V., Stegk, T., Matuschek, D., Ley, M. W. H. and Ramousse, S., The effect of forming stresses on the sintering of ultra-fine $Ce_{0.9}Gd_{0.1}O_{2-\delta}$ powders. *J. Eur. Ceram. Soc*., 2013, **33**, 1289-1296.

[34] Kaiser, A., Foghmoes, S., Chatzichristodoulou, C., Søgaard, M., Glasscock, J. A., Frandsen, H. L. and Hendriksen, P. V., Evaluation of thin film ceria membranes for syngas membrane reactors-preparation, characterization and testing. *J. Membr. Sci.*, 2011, **378**, 51-60.

[35] http://rsbweb.nih.gov/ij/.

[36] Ni, D. W., Esposito, V., Schmidt, C. G., Molla, T. T., Andersen, K. B., Kaiser, A., Ramousse, S. and Pryds, N., Camber evolution and stress development of porous ceramic bi-layers during co-firing. *J. Am. Ceram. Soc.*, 2013, **96**, 972-978.

[37] Rahaman, M. N., Sintering of ceramics. CRC press, 2007.

[38] Dutta, S. K. and Sprigge. R. M., Grain growth in fully dense ZnO. *J. Am. Ceram. Soc.*, 1970, **53**, 61-62.

[39] Kim, J. S., Rudkin, R. A., Wang, X. and Atkinson, A., Constrained sintering kinetics of 3YSZ films. *J. Eur. Ceram. Soc*., 2011, **31**, 2231-2239.

Figure Captions:

Fig. 1 Strain comparison of CGO10 pellet and tape as a function of sintering temperature at a heating rate of 1°C/min in the temperature range of 800-1250 °C. The inset is the linear strain rate of the correspondent plots.

Fig. 2 Relative densities evolution of porous CGO10 tape as a function of temperature at different heating rates in the temperature range of 800-1250 °C. Inset plots show the corresponding densification rates.

Fig. 3 Logarithm curves of $Ln(\mathrm{T}\frac{d\rho}{dt})$ against reciprocal sintering temperature for CGO10 tape at different relative densities

Fig. 4 Constructed MSC for sintering of porous CGO10 tape using activation energy of Q=440 kJ·mol^{-1} for the whole stage. The inset shows the mean residual square (MRS) as a function of activation energy.

Fig. 5 Determination of activation energy for densification of porous CGO10 tape by using Dorn's method

Fig. 6 SEM images of CGO10 tape sintered at 1250 °C/0h and 1250 °C/4h

Fig. 7 Variations of average grain size versus isothermal time at different temperatures

Fig. 8 Logarithm curves of $Ln(\mathrm{G}_t^{\,2}-\mathrm{G}_0^{\,2})$ against reciprocal sintering temperature of CGO10 tape, with apparent activation energy indicated

Fig. 9 Grain growth master curve for porous CGO10 tape

Densification and grain growth during sintering of porous $Ce_{0.9}Gd_{0.1}O_{1.95}$ tape cast layers: a comprehensive study on heuristic methods

De Wei Ni [*], Cristine Grings Schmidt, Francesca Teocoli, Andreas Kaiser, Kjeld Bøhm Andersen, Severine Ramousse, Vincenzo Esposito

Department of Energy Conversion and Storage, Technical University of Denmark, Frederiksborgvej 399, DK-4000 Roskilde, Denmark.

[*] Corresponding author: dwei@dtu.dk, Tel: +45 4677-5778, Fax: +45 4677-5858

Abstract:

The sintering behavior of porous $Ce_{0.9}Gd_{0.1}O_{1.95}$ (CGO10) tape cast layers was systematically investigated to establish fundamental kinetic parameters associated to densification and grain growth. Densification and grain growth were characterized by a set of different methods to determine the dominant sintering mechanisms and kinetics, both in isothermal and at constant heating rate (iso-rate) conditions. Densification of porous CGO10 tape is thermally activated with typical activation energy which was estimated around 440-470 $kJ \cdot mol^{-1}$. Grain growth showed similar thermal activation energy of ~427±22 $kJ \cdot mol^{-1}$ in the temperature range of 1100-1250 °C. Grain-boundary diffusion was identified to be the dominant mechanism in porous CGO10 tapes. Grain growth and densification mechanism were found strictly related in the investigated temperature range. Porosity acts as a grain growth inhibitor and grain boundary mobility in the porous body was estimated around 10^{-18}-10^{-16} $m^3 \cdot N^{-1} \cdot s^{-1}$ at the investigated temperature range.

Key Words: Sintering; Grain growth; CeO_2; Porosity; Grain boundary.

I. Introduction

Ceria is an important catalytic material that offers high stability, tolerance against harsh environments and electrical conductivity at high temperatures [1, 2]. Particularly, trivalent acceptor doped ceria (*e.g.* A^{3+}, where A is Gd, Sm, Dy *etc.*) has attracted interest for its potential as fast ionic conductor in electrochemical applications [3, 4]. Gadolinium doped ceria (CGO) is the best electrolyte material choice for intermediate temperatures solid oxide fuel cells (IT-SOFC) operating at 600 °C [5-7] and for flue gas purification electrochemical devices [8, 9]. Other applications are as barrier layers in SOFC [10] and oxygen transport membranes operating at high temperatures [11, 12]. Conventionally, the most used doping amounts of gadolinium in ceria are 10mol% and 20mol% (CGO10 and CGO20 for simplification). For most of these applications, CGO is applied as a thin dense layer on a porous support structure. However, highly porous layer allowing gas flow is necessary in catalytic and in gas purification devices. Independent on the final application, tape casting is a very versatile and cost effective large scale production technique [8, 10, 13]. Furthermore, sintering is of great importance for the final microstructure (*e.g.* density and grain size) since it induces most of the morphological transformations at high temperature.

In recent years, numerous models have been proposed for a computer simulation and prediction of sintering behavior. The models are based on constitutive laws of sintering and critically depend on the quality of the experimental input parameters [14-18]. The sintering mechanisms activation energy is a crucial input parameter. This can be derived from the constitutive laws by several methods and characterize densification and grain growth in different conditions such as iso-strain (iso-density) lines approach [17-24] and master sintering curve method (MSC) [25, 26] in iso-rate conditions or Dorn's method in iso-thermal conditions [20, 21, 27, 28]. Both the iso-strain (iso-density) lines approach and MSC method assume that microstructural evolution (both grain size and geometry) are dependent only on density for any given powder and green-body process. Iso-strain (iso-density) lines approach can give out the apparent activation energy evolutions at different densification levels in iso-rate conditions, while

MSC method seeks the best fitting energy value of the entire densification process. MSC is mostly reliable in the case that one diffusion mechanism is dominant in sintering process (*i.e.* constant activation energy) [25]. Conversely to the iso-strain (iso-density) lines approach and MSC method, the Dorn's method gives direct access to the densification activation energy [20, 21, 27, 28] by a series of incremental isothermal heating treatments. These methods have been widely used for CGO, especially for the characterization of dry pressed pellet samples sintering. Several values of activation energy have been reported extensively either for undoped or doped ceria using these methods [19, 24, 29-31]. However, with respect to the tape cast materials, a detailed characterization and investigation on the sintering kinetics and activation energy is still missing. This is probably due to the experimental complications related to the use of slurry-based samples, which present lower density (*i.e.* high porosity) at the green stage. Moreover, supercritical porosity is usually present for green density below 50% [32]. Supercritical porosity is stable in the material during sintering and it can greatly influence densification and grain growth. On the other hand, it has shown that different stress level in the shaping processing can actually influence the particles arrangement in the green body and thus the final densification during sintering [33]. The sintering behavior of low-density tapes is therefore expected to be different from the conventional dry pressing pellets.

In the present work porous CGO10 tape with low-green density relevant for electrolytes in flue gas purification devices, was prepared by tape casting. The densification and grain growth processes of the porous CGO10 tape during sintering were investigated experimentally by optical dilatometry and microscopy. Based on the achieved results, the activation energies for densification and grain growth were evaluated and compared using different approaches (iso-density lines approach, master sintering curve (MSC) method, as well as Dorn's method), which provided insight into the densification mechanisms. For comparison, the sintering behavior of CGO10 dry pressing pellet was also studied. More generally, this investigation provided a fundamental understanding for densification and grain growth activation energy evaluation by different methods in terms of porous tape cast layer.

II. Experimental procedures

2.1 Material and tape casting

$Ce_{0.9}Gd_{0.1}O_{1.95}$ with low surface area (12.8 m^2/g, Rhodia S.A., France) was used as starting materials. Two graphite pore formers (V-UF1 99.9, d_{50}: 2.6μm, Graphit Kropfmühl, Germany and SGB 10 L/99.9, d_{50}: 10μm, Graphit Kropfmühl, Germany) were used in order to obtain sufficient open porosity and pores with suitable shape and size (mainly in respect to use in flue gas purification devices), so that the pores could connect to each other very well. The amounts of the two graphite pore formers were ~4.8 wt% and 2.1wt%, respectively. The resulting powder mixture was dispersed in a methylehylketone and ethanol (MEKET) based suspension with polyvinyl-pyrrolidone (PVP) as dispersant and polyvinylbutyral (PVB) as binder [34]. The resulting slurry for tape casting was homogenized by ball milling for 72 hours. It was tape-casted on Mylar® foil at constant speed (20 cm/min) in a controlled environment with a blade clearance around 150 μm. The final thickness of the CGO10 tape was approximately 30 μm (green tapes after drying). The CGO green tape was tight rolled and pressed to obtain "bulky" sample of the thin layer which allowed dilatometry measurement. Final shapes of the samples were obtained by cutting the rolled tapes in cylindrical chips of about 5-8 mm in length and 3-5 mm in diameter.

2.2 Dilatometric measurement

Dilatometric measurements were performed by an optical dilatometer (TOMMI, Fraunhofer ISC, Würzburg, Germany). This allows following samples shape evolution during sintering by *in-situ* and non-contact, simply collecting the sequent images of the samples' silhouettes projected by a source of visible light onto a high definition camera [17, 23]. "Non-contact" measurement is critical for the tape casting layer due to its intrinsic poor mechanical properties before sintering. The complete thermal cycle including de-binding, pore former removal and sintering, was performed directly in the optical

dilatometer to avoid any possible stress on the samples. The de-binding cycle included a slow heating ramp at 0.33 °C/min step from room temperature to 400 °C, and an isothermal treatment step at 400 °C for 4h to ensure the binders removal. After binder burnout, the samples were fired at the same heating rate to 800°C and held for 2h to remove the graphite pore former. The samples were then heated to 1250 °C (after 800 °C) at heating rates of 0.33, 1 and 5 °C/min. Different heating rates were performed for the iso-density lines approach and the MSC method study. For the Dorn's method, the temperature increment was given at a step of 15 °C/min in a temperature range of 900-1080 °C in a sequence of 6 steps, with holding of 20 minutes at each step.

The linear strain (ε) was monitored *in situ* continuously during the heating and cooling cycles. Thermal expansion of the samples was corrected using the thermal expansion coefficient (TEC) determined from the cooling part of the shrinkage curve. The relative densities (ρ) as a function of temperature is calculated from the linear strain data assuming an isotropic shrinkage behavior:

$$\rho(T) = \rho_0 \exp(-3\varepsilon) \tag{1}$$

where ρ_0 is the relative density of green sample.

2.3 Microstructure and grain growth

To study the grain growth behaviour of the as-prepared CGO10 tape, the green samples were sintered at four different sintering temperatures with different holding time. Cross sections of the sintered samples were polished and thermally etched at temperatures 100 °C lower than their respective sintering temperatures for 0.5 h to reveal grain boundaries. And microstructures were observed using field emission scanning electron microscopy (FE-SEM, Supra, Carl Zeiss, Germany). The porosity and grain size after sintering were determined by post processing of the SEM images, using freeware software ImageJ® [35]. To reduce the error in the determination of porosity, at least ten images with hundreds of pores were taken

in random regions of the samples and used for the statistical analysis. The relative density was estimated as deduction of porosity. Average grain sizes of the sintered materials were determined by linear intercept method from at least 100 randomly selected grains.

III. Results and discussion

3.1 Comparison of sintering behavior between CGO10 dry pressing pellet and tape cast layer

To clarify the difference in the densification behavior between CGO10 dry pressing pellet and porous tape cast layer, the shrinkage of these two kinds of samples (prepared using identical starting powders) during sintering was studied and compared at first. **Fig. 1** shows the variations of shrinkage with temperature at a heating rate of 1°C/min in the temperature range of 800-1250 °C, the inset is the linear strain rate of the two samples. The strain curve of the CGO10 tape cast layer shows similar trend to that of the dry pressing pellet. However, CGO10 tape shows slower shrinkage behavior compared with the dry pressing pellet at lower temperature, whereas it becomes faster as temperature increases. Simultaneously, it can also be found that the temperature at which the CGO10 tape starts to shrink is a little higher compared to the dry pressing pellet. Their difference is shown more clearly in the strain rate plots inserted in **Fig. 1**. The CGO10 dry pressing pellet shows a higher strain rate at the temperature lower than ~950 °C, and achieves its highest shrinkage rate at about 1080 °C. Whereas the CGO10 tape has a faster strain rate in the temperature range of 950-1250 °C and achieves its highest shrinkage rate at about 1060 °C. This indicates that the densification of CGO10 tape is significantly enhanced compared with the dry pressing pellet at higher temperatures. The repeat of the dilatometric measurement shows good reproducibility for the tape cast samples. Pressed pellets samples can present different sintering behavior depending on the shaping techniques [33]. Therefore, it can be rest assured that the sintering behavior

difference between CGO10 pellet and tape is resulted from their intrinsic microstructural characteristics at the green stage.

Green density, particles and pores arrangement in green samples are important factors influencing mass diffusion during sintering. In this study, the green density of the CGO10 dry pressing pellet was estimated about 0.55 from the geometric shape after cold isostatic pressing. The relative density was about 0.40 for the CGO10 tape after de-binding and pore former removal. Green density for tapes was estimated by the dilatometry data considering the rolled sample isotropic and counting that the measured final relative density of the sample was at 0.63. As expected, the CGO10 dry pressing pellets exhibited a relatively lower onset temperature for densification, and showed a faster shrinkage rate at lower temperature. Normally, colloid processing (*e.g.* tape casting and slip casting) can obtain uniform microstructure with uniform particle arrangement and less agglomeration, compared to conventional powder processing (*e.g.* dry pressing). This can lead to faster shrinkage and higher densification. In another work, some of the authors of this paper have shown that different stress level in the shaping processing can actually influence the particles arrangement in the green body and thus the final densification during sintering. Particularly, it was demonstrated that high packing at the green stage cannot result in the higher final density in the case that the sintering shaping stress is high [33]. According to this result, it is confirmed that accurate analysis of the sintering kinetics of tape cast layer cannot be carried out on pressed pellet samples and original shaped samples must be investigated.

3.2 Determination of densification kinetics of CGO10 tape

3.2.1 TOMMI measurement of CGO10 tape during sintering at different heating rates

The strains during sintering of porous CGO10 tape cast layer were measured *in-situ* and non-contact using a thermo-optical measuring technique (optical dilatometer, TOMMI). The non-contact techniques allow following densification process during firing for samples of diverse shapes in a large

range of shape evolutions. The optical system in TOMMI is designed to project the sample shadow silhouette into a high resolution camera [17, 23]. This can register both swelling and shrinkage in a range of sizes and directions that conventional contact dilatometer cannot register. Optical dilatometry is particularly reliable for the characterization of tape-cast and slurry based samples, where high amount of organic component can lead to drastic change in the sample shape during the firing process [33, 36].

Based on the shrinkage strains *in situ* measured by TOMMI, the relative densities of porous CGO10 tapes sintered at different heating rates were calculated using Eq. (1). **Fig. 2** shows the variations of relative density with sintering temperature at different heating rates in the temperature range of 800-1250 °C. It can be seen that the relative density in **Fig. 2** increased continuously with the sintering temperature in the investigated sintering temperature range (800-1250 °C). The porous CGO10 tape starts to densify at about 850 °C and the onset temperature slightly increases as heating rate increases. Remarkable densification is observed at temperatures above 900 °C. The densification proceeds without the typical plateau of the final stage of the sintering, indicating that the residual porosity is not stable and it can be further reduced by firing at high temperatures. The porous CGO10 tape studied in this work was designed for flue gas purification. Therefore a large amount of graphite pore-former was added. After de-binding and pore-former removal, typical porous CGO10 tape reaches relative density of 0.40 (*i.e.* white density). The final relative density at 1250 °C at the heating rate of 0.33 °C/min is about 0.664. The sintering profile changed at different heating rates leading to final density of 0.626 and 0.607 at the heating rates of 1 and 5 °C/min, respectively. Porosity values of around 35% would fulfill the requirements of free passage of the gases through the flue gas purification devices, assuming that the most of the porosity is open and connected [8, 9]. According to results in **Fig. 2**, such a density locates at the early stage sintering for the investigated temperatures range [18].

The densification rates of the porous CGO10 tape during sintering were also evaluated from the time derivatives of the density curves (inset **Fig. 2**). Densification rate curves conveniently display samples sintering activity at different heating conditions. Particularly, the inset plots in **Fig. 2** show that

the densification rate increases with the sintering temperature, attaining a peak of activity and then decreasing with the temperature. Furthermore, as the heating rate increases, the maximum densification rate increases and shifts towards higher temperatures. The densification rates peaks are achieved at about 1010, 1060 and 1090 °C respectively as heating rate increases. These results are also consistent with those reported by He *et al* [19] on CGO10 pellets densification behavior.

3.2.2 Densification kinetics analysis based on constitutive laws

Shrinkage during sintering is driven by thermally activated forces generated in the porous compacts by interface energy minimization between particles, pores, and grains. Surface diffusion, grain boundary diffusion and volume diffusion are the three main thermally activated mechanisms for mass transfer, which can occur simultaneously during sintering [37]. In the constitutive laws for densification, the densification rate is expressed as a function of activation energy (Q), which includes all the mechanisms generated during sintering [16, 17]. The strain rate is usually described by the formula:

$$-\frac{d\varepsilon}{dt}=\frac{1}{3\rho}\frac{d\rho}{dt}=\frac{C_1(\rho)\gamma D}{kTG^n}=\frac{C_1(\rho)\gamma D_0}{kTG^n}\exp(-\frac{Q}{RT}) \tag{2}$$

where ε is the true strain, ρ is relative density, t is time, C_1 is a constant depending on microstructure, γ is the solid-gas interface energy, D is the diffusion coefficient, Q is the apparent activation energy for diffusion mechanism leading to densification, R is the gas constant, k is Boltzmann constant, T is absolute temperature, G is mean grain size, n is a parameter depending on mechanism (3 for volume diffusion and 4 for grain boundary diffusion). According to the Eq. (2) the densification is thus function of density (porosity) and of some simplified microstructural constants (C_1, n) and grain size (G). However, grain size and porosity change with temperature and individual mechanisms cannot be identified by this approach. Nevertheless, such assumptions are convenient for the estimation of the activation energy of the

whole process, especially when sintering is strongly affected by a dominant mechanism. This is the case of doped ceria which is known to be limited by dominant grain boundary solute drag diffusion [29, 30].

(1) iso-strain (iso-density) lines approach

Rearranging and taking the logarithm of both sides of Eq. (2), the following equations can be obtained:

$$\ln(-T\frac{d\varepsilon}{dt}) = -\frac{Q}{R}\frac{1}{T} + \ln(\frac{C_1(\rho)\gamma D_0}{k}) - n\ln G \tag{3}$$

$$\ln(T\frac{d\rho}{dt}) = -\frac{Q}{R}\frac{1}{T} + \ln(\frac{3\rho C_1(\rho)\gamma D_0}{k}) - n\ln G \tag{4}$$

Logarithmic curves of $ln(-\mathrm{T}\frac{d\varepsilon}{dt})$ or $ln(\mathrm{T}\frac{d\rho}{dt})$ as a function of the reciprocal absolute temperature (*1/T*) measured during sintering of green compacts with different constant heating rates can be plotted according Eqs. (3) or (4). Then, points of equal strain (density) on different shrinkage curves can be connected to form so-called iso-strain (iso-density) lines. With the same densification level, the grain sizes are usually identical. Especially in the present work, the effect of grain growth is very limited in the studied density range (ρ<0.7). Therefore, straight lines could be obtained for the iso-strain (iso-density) lines respectively. From the slopes, the activation energy *Q* for densification can be calculated for the respective iso-strain (iso-density) conditions [17, 19-23].

Fig. 3 shows the corresponding plots for the evaluation of activation energy for densification of porous CGO10 tape based on the iso-density lines approach. As expected, the evaluation with the model described above leads to straight iso-density lines for all the investigated density values. Correlation coefficients for all the linear fitting in **Fig. 3** are higher than 0.98. Moreover, all the fitted lines are almost parallel to each other, indicating an independency of the activation energy on the relative density in the analyzed densification regime. The activation energy for densification in the investigated density range

(0.46-0.60) is evaluated to be 470±31 kJ·mol^{-1}. Chen [30] reported that the activation energy for densification of pure ceria and 1% gadolinium oxide doped ceria pellets in air is 6.16 eV (~593 kJ·mol^{-1}) and 4.66 eV (~449 kJ·mol^{-1}) respectively, and Jud *et al* [24] reported that the activation energy for densification of CGO20 pellet is 4.70±0.32 eV (~453±31 kJ·mol^{-1}) in the relative density range of 0.65-0.90. Therefore, the determined activation energy for densification of porous CGO10 tape, at the early-stage of the sintering, is comparable to those reported for dry pressing pellets in literature.

The estimation of grain size evolution with the temperature for the calculation of the densification activation energy in Eq. (2) can be theoretically distinguished from the densification mechanisms by evaluating the grain growth exponent *n*. Rearranging and taking the logarithm on both sides of Eq. (2), and including grain growth during sintering, a new formula gives the necessary equation for the determination of the activation energy:

$$\ln(TG^n \frac{d\rho}{dt}) = -\frac{Q}{R}\frac{1}{T} + \ln(\frac{3\rho C_1(\rho)\gamma D_0}{k}) \tag{5}$$

However, fits with low errors can be obtained for both *n* equals to 3 (volume diffusion) and 4 (grain boundary diffusion). And the activation energy exhibits in the case *n*=3 (~436±31 kJ·mol^{-1}) slightly lower value than the one for *n*=4 (~461±26 kJ·mol^{-1}). Volume diffusion normally exhibits higher activation energy than grain boundary diffusion, but diffusion in the case of solute drag mechanism at grain boundary can result highly energetic [30]. However, the adopted method does not allow distinguishing the densification mechanisms. This limitation has also been reported for sintering models based on the constitutive law for other systems [24, 30]. Other limitations are the relatively poor resolution of the applied plotting method, the constitutive scattering of dilatometric data, and the limiting assumption that C_1 is a constant with the temperature.

(2) Master sintering curve (MSC)

Master sintering curve (MSC) is another simple yet powerful approach to describe the sintering process [25, 26]. The concept of a MSC is based on the premise that the density of a sintering body is a unique function of its thermal history (*i.e.* all thermal histories can be reduced to a common relationship with relative density). Eq. (2) can be rearranged and integrated as follows:

$$\frac{k}{\gamma D_0}\int_{\rho_0}^{\rho}\frac{G^n}{3\rho C_1(\rho)}d\rho=\int_0^t\frac{1}{T}\exp(-\frac{Q}{RT})dt \tag{6}$$

$$\Phi(\rho)\equiv\frac{k}{\gamma D_0}\int_{\rho_0}^{\rho}\frac{G^n}{3\rho C_1(\rho)}d\rho \tag{7}$$

$$\Theta(t,T(t))\equiv\int_0^t\frac{1}{T}\exp(-\frac{Q}{RT})dt \tag{8}$$

In such a simplification, it can be found that the $\Phi(\rho)$ is a microstructure-related function, whereas $\Theta(t, T(t))$ depends only on Q and the time-temperature profile. Differently from the iso-density method, no microstructural parameters directly appear in the equations in MSC. The constants used in Eq. (2) are thus "reduced" to a general microstructural function, which includes all the possible microstructural evolutions as effect of the densification during sintering. By the MSC method, the relationship between the relative density ρ and $\Theta(t, T(t))$ is defined and possible solutions of the Eq. (8) are considered to estimate the activation energy of the dominant phenomena. The value of activation energy that yields the minimum mean residual square (MRS) is thus selected for the construction of MSC. Subsequent iterations allow for the calculation of densification curves for arbitrary time-temperature cycles. Vice versa, the time-temperature cycle can be calculated which provides prescribed densification rates.

In order to plot the master sintering curve, relative density ρ obtained at different heating rates is plotted against $\Theta(t, T(t))$ and the value of Q is adjusted where data fall on a single curve. The best fit is determined by minimizing the MRS deviation function:

$$\Delta(\ln(\Theta)) = \int_{\rho_0}^{\rho_f} \frac{(\sum_{i=1}^{N}(\ln(\Theta_i) - \ln(\Theta_{av}))^2)^{\frac{1}{2}}}{N(\rho_0 - \rho_f)} d\rho \tag{9}$$

where the summation is over the different heating rates, ρ_0 and ρ_f are the green and final densities. **Fig. 4** shows the MSC of porous CGO10 tape and inset shows MRS deviation function plotted against Q with minimum value of the best fit at 440±20 kJ·mol^{-1}. This activation energy value is in good agreement with the results from the iso-density lines method shown in **Fig. 3**. Using this value of Q= 440 kJ·mol^{-1}, the MSC for sintering of porous CGO10 tape was constructed, as shown in **Fig. 4**. It can be found that an excellent fitting was established based on the three densification curves in **Fig. 2**. The satisfactory construction of MSC reveals that the assumption for MSC establishment is satisfied in the present work. Limitations in using MSC approach are usually registered where sintering is a well-defined sequence of different mechanisms. In such cases the MSC can result difficult at the different level of densification [25]. Therefore, the microstructural evolution (both grain size and geometry) in porous CGO10 tape-cast sample are dependent mainly on density for the given powder and green body process, and most likely one dominant diffusion mechanism is occurring in the sintering process.

(3) Dorn's method

Conversely to the other methods, the Dorn's method gives direct access to the densification activation energy [20, 21, 27, 28] by a series of incremental isothermal heating treatments. Such an approach is commonly used to measure the activation energy of creep phenomena, and it thus can also be used to study sintering. By the Dorn's method, the isothermal strain rate is recorded firstly at a temperature T_1 for a sintering time t, then, following a temperature increment made as rapid as possible, the same recording is made at a temperature T_2, slightly higher than T_1. In such conditions, it can be assumed that the microstructural state remains unchanged during the temperature increment, and then the following equality can be obtained:

$$(\varepsilon)_{end\ step\ T_1} = (\varepsilon)_{beginning\ step\ T_2} \tag{10}$$

From Eq. (2), the ratio between the corresponding strain rates $\dot{\varepsilon} = \frac{d\varepsilon}{dt}$ can be expressed as:

$$\frac{\dot{\varepsilon}_2}{\dot{\varepsilon}_1} = \frac{T_1}{T_2} \exp\left(\frac{-Q}{R} (\frac{1}{T_2} - \frac{1}{T_1}) \right) \tag{11}$$

The densification activation energy is then deduced from:

$$Q = \frac{RT_1T_2}{T_2 - T_1} \ln\left(\frac{T_2\dot{\varepsilon}_2}{T_1\dot{\varepsilon}_1} \right) \tag{12}$$

An important assumption is that the microstructural state remains unchanged during the temperature increment. However, this may not always be the case during isothermal experiments especially at high densification levels. As well, isothermal holding may influence the sintering behavior at subsequent sintering steps as sintering proceeds. It is hence important that a short isothermal holding is used to reduce its influence on the subsequent sintering steps, while it must still be long enough to achieve thermal equilibrium at every isothermal step. The method better suits the early stage of sintering and an appropriate temperature interval is recommended to reduce the possible microstructural change during the temperature increment. For the porous CGO10 samples, the temperature increment was given at a step of 15 °C/min and an interval 30 °C from 900 °C to 1080 °C, and a holding of 20 minutes at each step was used. **Fig. 5** shows the determined activation energy for densification of porous CGO10 tape for each temperature step using Dorn's method. It was evaluated to be 453±27 kJ·mol^{-1}. This is again in good agreement with the results from the iso-density lines and MSC methods.

Comparing the results obtained from different methods, some simple considerations can be done. The three methods are based on the characterization of densification, as a function of the linear strain, by dilatometry. As a consequence, the accuracy of the data acquisition is crucial especially for those samples, as slurry-based ones, which can present drastic shape evolution during firing. In the iso-rate conditions,

the MSC gives a "best-fitting" energy value of the overall thermally activated phenomena while the iso-density lines approach gives out a series of activation energy at respective densification levels. Such values in the porous CGO tape samples, at the investigated density range (0.47-0.60), resulted almost constant. The Dorn's method also gives as result the values of activation energy at each thermal step. However, these resulted slightly different at the different steps, ranging from 417 to 479 kJ/mol. Particularly, **Fig. 5** shows that CGO10 tapes present a peak of thermal activation energy at temperatures between 950 and 1050 °C. Such a result is consistent with data in **Fig. 2** which shows a critical activity of sintering activity as function of the temperature. Although, the variation of the determined activation energy in the studied densification range is limited, the Dorn's method seems to represent in a better detail the thermal diffusivity in the sample than a representation limited to the level of densification. This can be explained by the fact that diffusive phenomena are better described by the thermal energy level than on the microstructure, especially when this is evolving in a narrow range of density and porosity variations.

Despite such differences, results showed that various heating cycles for the studied porous CGO10 tape can be described by the same MSC using constant thermal activation energy. It is proved that all the values of activation energy calculated by the three different methods match with each other quite well, no matter whether taken in iso-rate or iso-thermal conditions. This indicates that the assumptions for these methods, such as microstructure evolution during sintering only dependent on density, microstructural state unchanged during temperature increment in Dorn's method, *etc*. are basically correct in the present study. It also indicates that the whole investigated sintering process was dominated by a same diffusion mechanism. Such individual mechanism, however, cannot be distinguished by dilatometry and a direct microstructural characterization is needed.

3.3 Determination of grain growth kinetics of CGO10 tape

The above methods give out the apparent densification activation energy only based on the geometry (*i.e.* strain or density) evolution during sintering, which do not refer to any particular microstructures. However, the driving force in sintering is related to the microstructural features because it depends mainly on the surface energy at the grain boundaries and pore/grain interface. The grain growth of porous CGO10 tape during early stage sintering was also investigated to clarify the relation between microstructure and densification in the sintering kinetics. As an illustration, high resolution SEM images of CGO10 tape sintered at 1250 °C/0h and 1250 °C/4h are shown in **Fig. 6**.

The average grain size, *G*, was evaluated from the SEM images and **Fig. 7** displays the variations of grain size versus isothermal time at different temperatures. This shows that the grain size increases with sintering proceeds for all the investigated CGO10 tapes at different heating temperatures. Grain growth is very slow for the CGO10 samples sintered at 1100-1200 °C, which becomes faster for the samples sintered at 1250 °C. This is expected in CGO because the high dopant level constrains the growth by solute drag effect especially at low temperatures [30]. However, compared to the dry pressing pellets, the grain growth in the investigated porous CGO10 tape in the initial stage of sintering is very limited overall [19, 31], indicating a certain inhibition of the sintering process due to the large porosity in the samples. The latter is expected especially where supercritical porosity (stable) is present in the material [32, 37]. Although in CGO porous tapes final stage of the sintering was not achieved, both dilatometry (see, **Fig. 1**) and microscopy analysis (not shown here) suggested that supercritical porosity induced by use of graphite pore-former was pretty high at around 20-30 % of the total volume.

Normally, grain growth kinetics is analyzed under isothermal conditions from grain size vs. time curves (**Fig. 7**), in accordance with the well-known grain growth kinetics equation: [31, 38]

$$G_t^{\,m} - G_0^{\,m} = Kt = K_0 t \exp\left(-\frac{Q_g}{RT}\right) \tag{13}$$

where G_t is the average grain size at time t, G_0 is the initial grain size, m is the kinetic grain growth exponent typically between 2 and 4, K is a rate constant, K_0 is a pre-exponential constant, Q_g is the

apparent activation energy for grain growth, R is the gas constant and T is the absolute temperature. The kinetic grain growth exponent m for CGO was assumed to be 2 from Chen *et al* [30]. And therefore Eq. (13) can also be rewritten as:

$$Ln(G_t^{\,2} - G_0^{\,2}) = LnK_0 + Lnt - \frac{Q_g}{RT} \tag{14}$$

Fig. 8 shows the corresponding plots for the evaluation of activation energy for grain growth based on Eq. (14). It is shown that data are well fitted in by linear functions fitting and the activation energy for grain growth of CGO10 tape was evaluated by the slope to be 427±22 kJ·mol^{-1}. Correlation coefficients for all the linear fitting in **Fig. 8** are higher than 0.99. The pre-exponential constant K_0 was also calculated, with a value of 0.04 m^2·s^{-1}, which represents the grain growth rate to some extent. The fitting of grain growth exponent m equals to 3 and 4 was also conducted in this work, but the linear regression was unacceptable. This suggests that the assumption of m=2 is reasonable and grain growth of the porous CGO10 tape proceeds predominantly through grain boundary diffusion mechanism [30, 31]. It is also found that the evaluated activation energy for grain growth is very close to that determined for densification of CGO10 tape. Therefore, we can conclude that the densification processes of porous CGO10 tape in the early stage of sintering are dominated by the same diffusion mechanism.

Grain growth kinetics Eq. (13) can also be rewritten as [29, 30]:

$$G_t^{\,2} - G_0^{\,2} = 2M\gamma(t - t_0) \tag{15}$$

where M is the grain boundary mobility, γ is grain boundary energy. From the grain growth kinetics analyzed above, grain boundary mobility can be evaluated. In the analysis of the sintering processes, the grain boundary energy of the material is generally taken constant. For doped-ceria systems grain boundary energy is $\gamma \approx 0.3$ J·m^{-2} [29]. The grain boundary mobility for the porous CGO10 tape was calculated about 10^{-18}-10^{-16} m^3·N^{-1}·s^{-1} in the investigated temperature range (1100-1250 °C), which is estimated to be around 1-2 order of magnitude smaller than the corresponding dry pressing pellet [29].

This confirms that porosity acts as grain growth inhibitor during sintering. The forces driving the sintering are generated by energy minimization processes at the surface of particles and grains. Such phenomena are carried out via mass diffusion mechanisms and lead to spontaneous contacting, adhesion, densification and growth of the particles. High porosity can decrease the chance of particle contact, and grain boundary mobility is therefore slowed, which leads to the slower grain growth for the investigated porous CGO10 tape.

Similarly to the MSC, we can also define:

$$\Theta_g \equiv K_0 t \exp(-\frac{Q_g}{RT}) \tag{16}$$

Therefore, Eq. (13) can be rewritten as:

$$G_t^{\,2} - G_0^{\,2} = \Theta_g \tag{17}$$

The relationship between G_t and Θ_g can be regarded as a grain growth master curve [39]. Based on the evaluated pre-exponential constant K_0 and activation energy Q_g for grain growth, the grain growth master curve for sintering of porous CGO10 tape was constructed, as shown in **Fig. 9**. Our experimental measurements for CGO10 tape sintered at different temperatures and times are also shown in **Fig. 9**, well fitted to the constructed grain growth master curve.

V. Conclusion

Compared to dry pressing pellet, the porous CGO10 tapes showed different densification behavior due to their different green density and particle arrangement. This work investigated the densification and grain growth kinetics in the early-stage sintering of porous CGO10 tape. The sintering kinetics and activation energy for densification were determined employing three different methods: iso-density lines approach, master sintering curve (MSC), and the Dorn's method. The iso-density lines

approach and Dorn's method gave out a series of activation energy at respective densification levels, whereas the variation of the determined values in the investigated densification range is very limited. For the MSC method, constant activation energy was determined for the entire sintering process. All the three methods produced similar kinetics results with densification activation energy of around 440-470 $kJ \cdot mol^{-1}$. This indicated that the whole investigated sintering process is dominated by a unique diffusion mechanism. Moreover, the activation energy for grain growth was evaluated to be ~427±22 $kJ \cdot mol^{-1}$ in the temperature range 1100-1250 °C and the grain growth master curve was constructed. It is indicated that both the densification and grain growth processes for porous CGO10 tape are dominated by grain boundary diffusion mechanism. The determined activation energy for densification energy and grain growth of porous CGO10 tape is comparable to those values reported for gadolinium oxide doped ceria dry pressing pellets in literature. However, due to the high porosity, the grain boundary mobility for porous CGO10 tape (10^{-18}-10^{-16} $m^3 \cdot N^{-1} \cdot s^{-1}$) was estimated around 1-2 order of magnitude smaller than the corresponding dry pressing pellet in the investigated temperature range, which led to the slower grain growth behaviour in porous CGO10 tape.

Acknowledgement:

The authors would like to acknowledge the support of the Scientific Research Councils on Technology and Production Sciences (FTP) (Contract No. 09-072888, OPTIMAC), which is part of the Danish Council for Independent Research (DFF). Discussions with Karsten Agersted and Nini Pryds from DTU Energy Conversion and Storage Department are highly appreciated.

References:

[1] Mogensen, M., Sammes, N. M. and Tompsett, G. A., Physical, chemical and electro-chemical properties of pure and doped ceria. *Solid State Ionics*, 2000, **129**, 63-94.

[2] Kleinlogel, C. and Gauckler, L. J., Sintering and properties of nanosized ceria solid solutions. *Solid State Ionics*, 2000, **135**, 567-573.

[3] Wang, S., Kobayashi, T., Dokiya, M. and Hashimoto, T., Electrical and ionic conductivity of Gd-doped ceria. *J. Electrochem. Soc*., 2000, **147**, 3606-3609.

[4] Gorte, R. J., Kim, H. and Vohs, J. M., Novel SOFC anodes for the direct electrochemical oxidation of hydrocarbon. *J. Power Sources***,** 2001, **106**, 10-15.

[5] Meier, L. P., Urech, L. and Gauckler, L. J., Tape casting of nanocrystalline ceria gadolinia powder. *J. Eur. Ceram. Soc.*, 2004, **24**, 3753-3758.

[6] Cheng, J., Zha, S., Fang, X., Liu, X. and Meng, G., On the green density, sintering behavior and electrical property of tape cast $Ce_{0.9}Gd_{0.1}O_{1.95}$ electrolyte films. *Mater. Res. Bull*., 2002, **37**, 2437-2446.

[7] Atkinson, A. and Selcuk, A., Mechanical behaviour of ceramic oxygen ionconducting membranes. *Solid State Ionics*, 2000, **134**, 59-66.

[8] Christensen, H. and Rak, Z. S., A novel diesel particulate converter. *Catal. Today*, 2002, **75**, 451-457.

[9] He, Z., Andersen, K. B., Keel, L., Nygaard, F. B., Menon, M. and Hansen, K. K., Processing and characterization of porous electrochemical cells for flue gas purification. *Ionics*, 2009 **15**, 427-431.

[10] Simner, S. P., Anderson, M. D., Engelhard, M. H. and Stevenson, J.W., Degradation mechanisms of La-Sr-Co-Fe-O_3 SOFC cathodes. *Electrochem. Solid State Lett.*, 2006, **9**, A478-481.

[11] Steele, B. C. H., Oxygen-transport and exchange in oxide ceramics, *J. Power Sources*, 1994, **49**, 1-14.

[12] Ji, Y., Kilner, J. A. and Carolan, M. F., Electrical conductivity and oxygen transfer in gadolinia-doped ceria (CGO)-$Co_3O_{4-\delta}$ composites. *J. Eur. Ceram. Soc.*, 2004, **24**, 3613-3616.

[13] Klemensø, T., Menon, M. and Ramousse, S., Low toxicity binder systems for tape cast $Ce_{0.9}Gd_{0.1}O_{1.95}$ laminates. *Ceram. Int.*, 2010, **36**, 773-780.

[14] Riedel, H., Zipse, H. and Svoboda, J., Equilibrium pore surfaces, sintering stresses and constitutive equations for the intermediate and late stages of sintering. II. Diffusional densification and creep. *Acta Metall. Mater.*, 1994, **42**, 445-452.

[15] Camacho-Montes, H., Garcia-Casillas, P. E., Rodriguez-Ramos, R., Fuentes-Montero, M. E. and Fuentes-Cobas, L. E., Simulation of the stress-assisted densification behavior of powder compact: effect of constitutive law. *J. Am. Ceram. Soc.*, 2008, **91**, 836-845.

[16] Rahaman, M. N., *Sintering of Ceramics*, CRC Press, Boca Raton, 2008.

[17] Raether, F. and Horn, P. S., Investigation of sintering mechanisms of alumina using kinetic field and master sintering diagrams. *J. Eur. Ceram. Soc*., 2009, **29**, 2225-2234.

[18] He, Z. M. and Ma, J., Constitutive modeling of the densification of micron-grain-sized alumina ceramics. *Philos. Mag.*, 2003, **83**, 1889-1916.

[19] He, Z. M., Yuan, H., Glasscock, J. A., Chatzichristodoulou, C., Phair, J. W., Kaiser, A. and Ramousse, S., Densification and grain growth during early-stage sintering of $Ce_{0.9}Gd_{0.1}O_{1.95-\delta}$ in a reducing atmosphere. *Acta. Mater*., 2010, **58**, 3860-3866.

[20] Dehaudt, P., Bourgeois, L. and Chevrel, H., Activation energy of UO_2 and UO_{2+x} sintering. *J. Nucl. Mater.*, 2001, **299**, 250-259.

[21] Lahiri, D., Ramana Rao, S. V., Hemantha Rao, G. V. S. and Srivastava, R. K., Study on sintering kinetics and activation energy of UO_2 pellets using three different methods. *J. Nucl. Mater.*, 2006, **357**, 88-96.

[22] Wang, J. and Raj, R., Estimate of the activation energies for boundary diffusion from rate-controlled sintering of pure alumina, and alumina doped with zirconia or titania. *J. Am. Ceram. Soc.*, 1990, **73**, 1172-1175.

[23] Raether, F., Current state of in-situ measuring methods for the control of firing processes. *J. Am. Ceram. Soc.*, 2009, **92**, S146-152.

[24] Jud, E., Huwiler, C. B. and Gauckler, L. J., Sintering analysis of undoped and cobalt oxide doped ceria solid solutions. *J. Am. Ceram. Soc.*, 2005, **88**, 3013-3019.

[25] Su, H. H. and Johnson, D. L., Master sintering curve: a practical approach to sintering. *J. Am. Ceram. Soc.*, 1996, **79**, 3211-3217.

[26] Hansen, J. D., Rusin, R. P., Teng, M. H. and Johnson, D. L., Combined-stage sintering model. *J. Am. Ceram. Soc.*, 1992, **75,** 1129-1135.

[27] Dorn, J. E., pp. 255-83 in Creep and Recovery. Edited by R. Maddin. American Society for Metals, Cleveland, Ohio, 1957.

[28] Bacmann, J. J. and Cizeron, G., Dorn method in the study of initial phase of uranium dioxide sintering. *J. Am. Ceram. Soc*., 1968, **51**, 209-212.

[29] Chen, P. L. and Chen, I. W., Role of defect interaction in boundary mobility and cation diffusivity of CeO_2. *J. Am. Ceram. Soc.*, 1994, **77**, 2289-2297.

[30] Chen, I. W., Grain boundary kinetics in oxide ceramics with the cubic fluorite crystal structure and its derivatives. *Interf. Sci.*, 2000, **8**, 147-156.

[31] Li, J. G., Ikegami, T. and Mori, T., Low temperature processing of dense samarium-doped CeO_2 ceramics: sintering and grain growth behaviors. *Acta. Mater*., 2010, **52**, 2221-2226.

[32] Chen, P. L. and Chen, I. W., Sinering of fine oxide powders: I, microstructural evolution. *J. Am. Ceram. Soc.*, 1996, **79**, 3129-3141.

[33] Glasscock, J. A., Esposito, V., Foghmoes, S. P. V., Stegk, T., Matuschek, D., Ley, M. W. H. and Ramousse, S., The effect of forming stresses on the sintering of ultra-fine $Ce_{0.9}Gd_{0.1}O_{2-\delta}$ powders. *J. Eur. Ceram. Soc*., 2013, **33**, 1289-1296.

[34] Kaiser, A., Foghmoes, S., Chatzichristodoulou, C., Søgaard, M., Glasscock, J. A., Frandsen, H. L. and Hendriksen, P. V., Evaluation of thin film ceria membranes for syngas membrane reactors-preparation, characterization and testing. *J. Membr. Sci.*, 2011, **378**, 51-60.

[35] http://rsbweb.nih.gov/ij/.

[36] Ni, D. W., Esposito, V., Schmidt, C. G., Molla, T. T., Andersen, K. B., Kaiser, A., Ramousse, S. and Pryds, N., Camber evolution and stress development of porous ceramic bi-layers during co-firing. *J. Am. Ceram. Soc.*, 2013, **96**, 972-978.

[37] Rahaman, M. N., Sintering of ceramics. CRC press, 2007.

[38] Dutta, S. K. and Sprigge. R. M., Grain growth in fully dense ZnO. *J. Am. Ceram. Soc.*, 1970, **53**, 61-62.

[39] Kim, J. S., Rudkin, R. A., Wang, X. and Atkinson, A., Constrained sintering kinetics of 3YSZ films. *J. Eur. Ceram. Soc*., 2011, **31**, 2231-2239.

Figure Captions:

Fig. 1 Strain comparison of CGO10 pellet and tape as a function of sintering temperature at a heating rate of 1°C/min in the temperature range of 800-1250 °C. The inset is the linear strain rate of the correspondent plots.

Fig. 2 Relative densities evolution of porous CGO10 tape as a function of temperature at different heating rates in the temperature range of 800-1250 °C. Inset plots show the corresponding densification rates.

Fig. 3 Logarithm curves of $Ln(\mathrm{T}\frac{d\rho}{dt})$ against reciprocal sintering temperature for CGO10 tape at different relative densities

Fig. 4 Constructed MSC for sintering of porous CGO10 tape using activation energy of Q=440 kJ·mol^{-1} for the whole stage. The inset shows the mean residual square (MRS) as a function of activation energy.

Fig. 5 Determination of activation energy for densification of porous CGO10 tape by using Dorn's method

Fig. 6 SEM images of CGO10 tape sintered at 1250 °C/0h and 1250 °C/4h

Fig. 7 Variations of average grain size versus isothermal time at different temperatures

Fig. 8 Logarithm curves of $Ln(\mathrm{G}_t^{\,2}-\mathrm{G}_0^{\,2})$ against reciprocal sintering temperature of CGO10 tape, with apparent activation energy indicated

Fig. 9 Grain growth master curve for porous CGO10 tape

Fig. 1.tif
Click here to download high resolution image

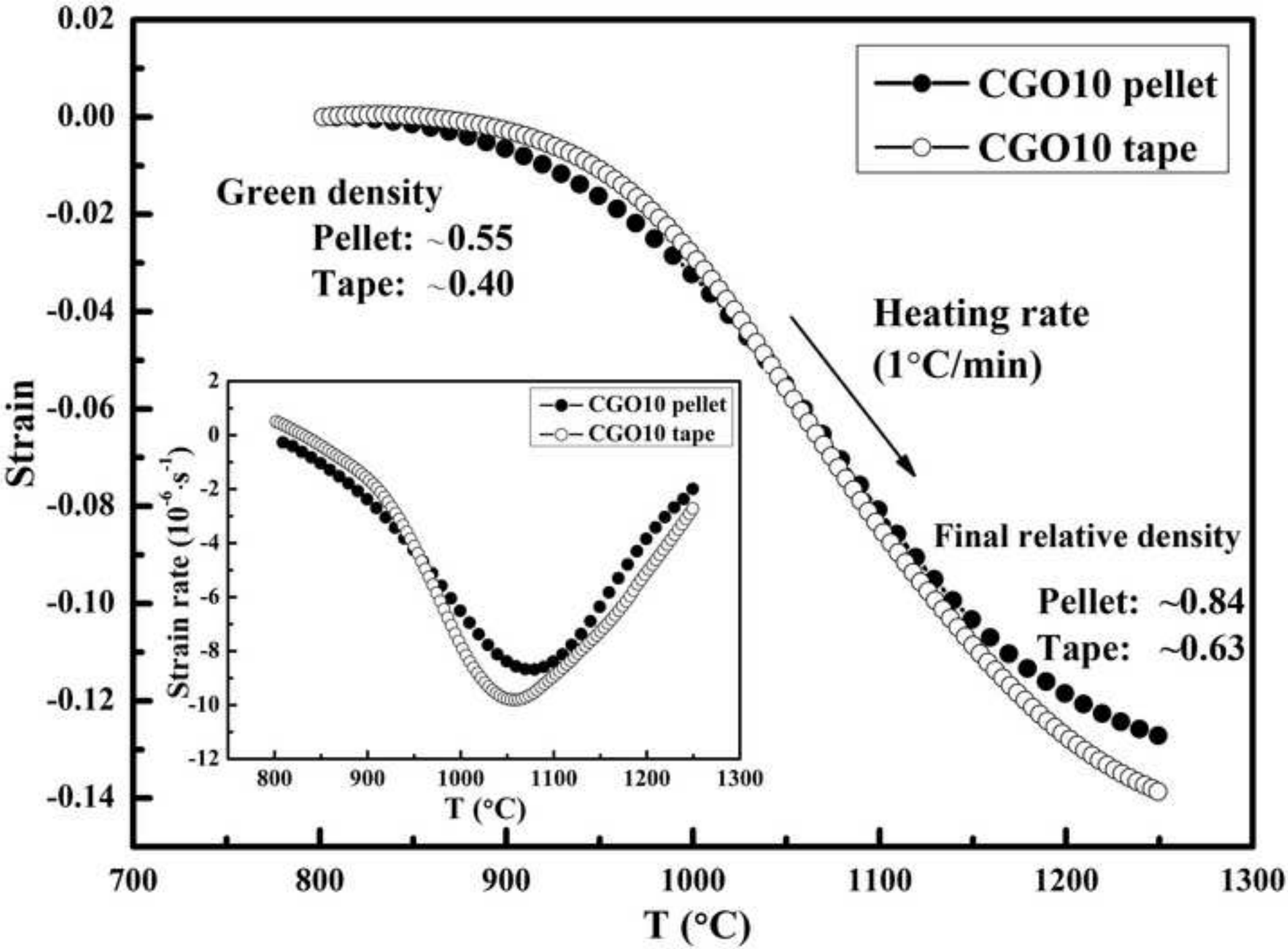

Fig. 2.tif
Click here to download high resolution image

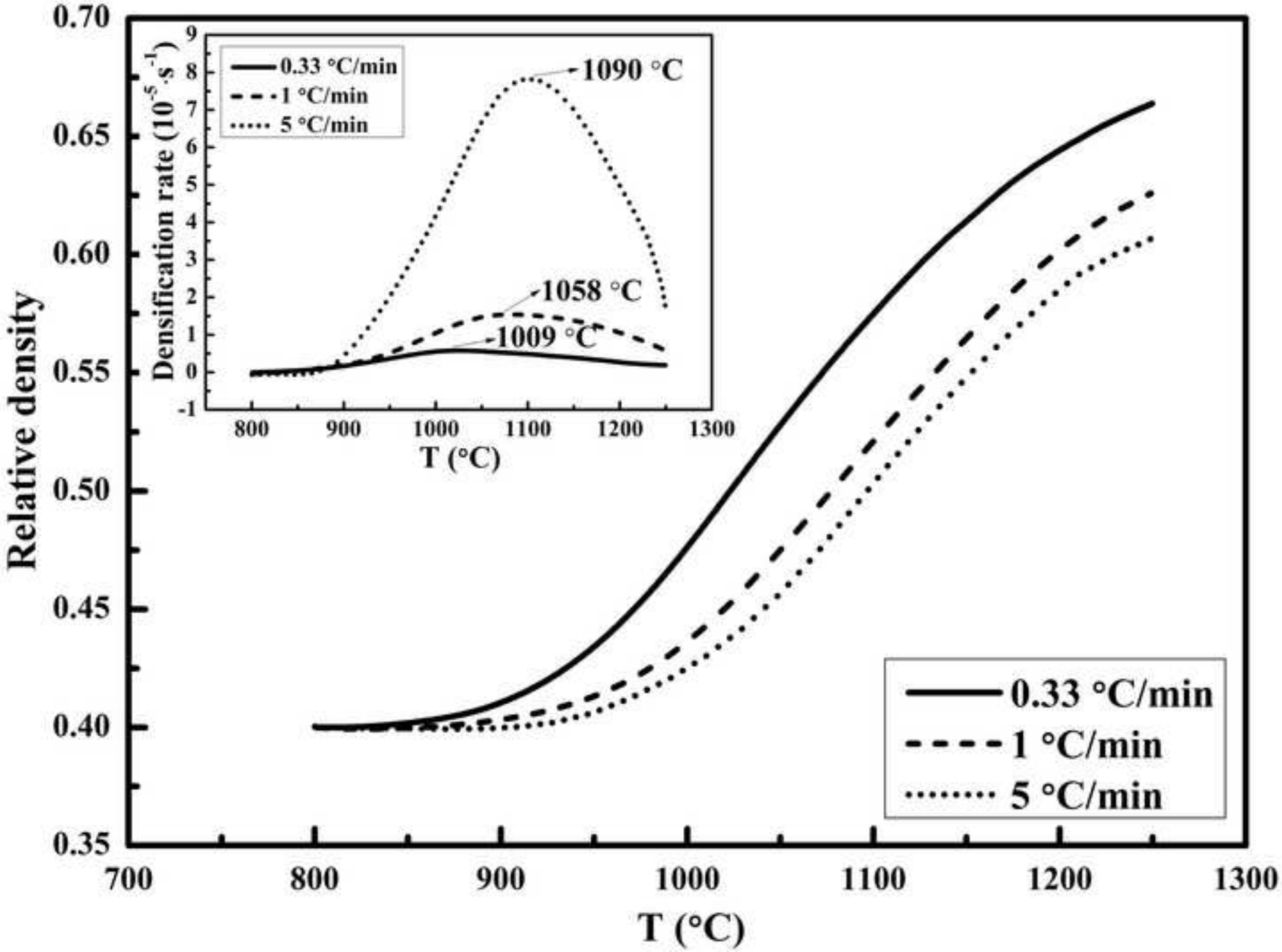

Fig. 3.tif
Click here to download high resolution image

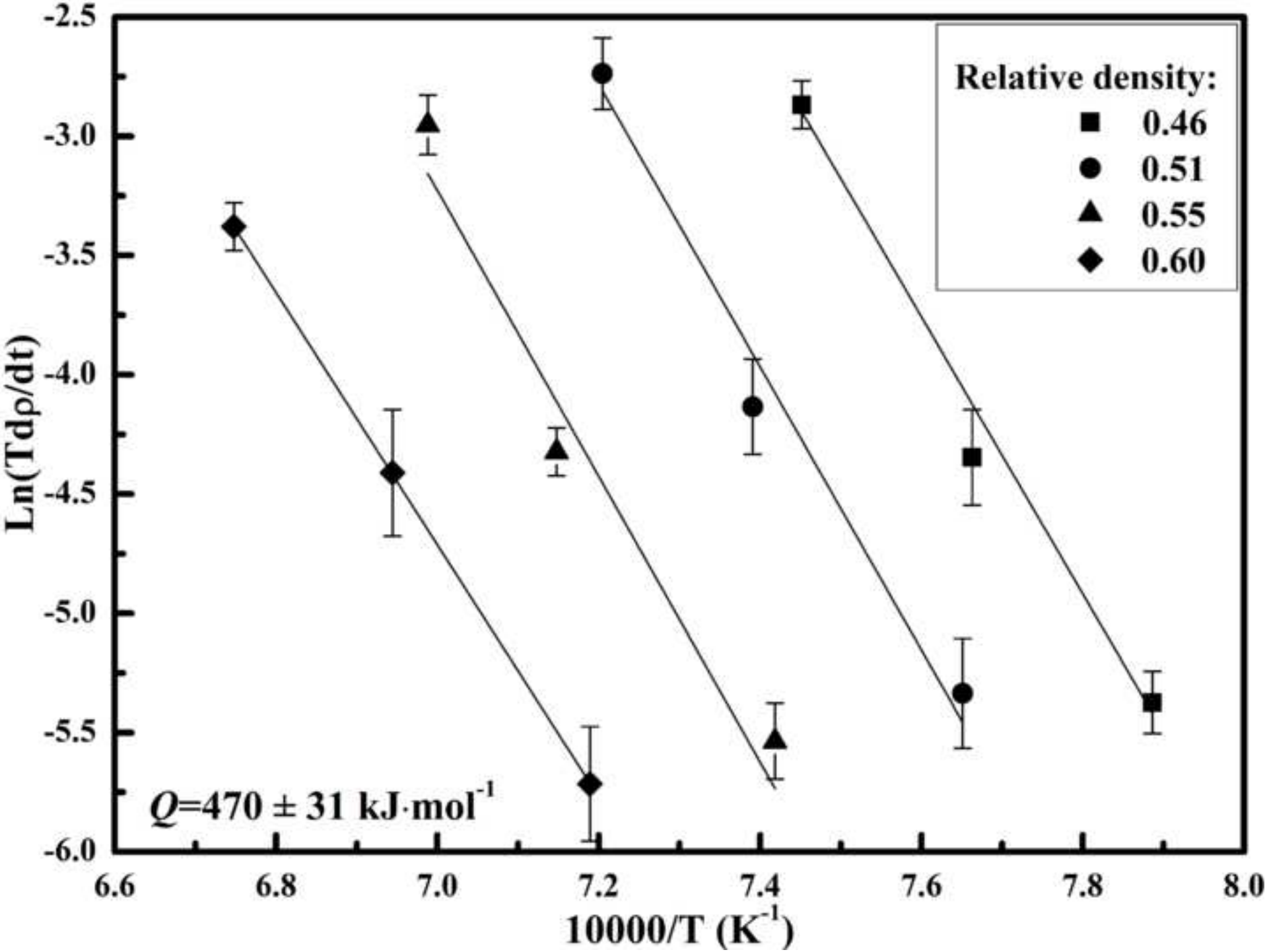

Fig. 4.tif
Click here to download high resolution image

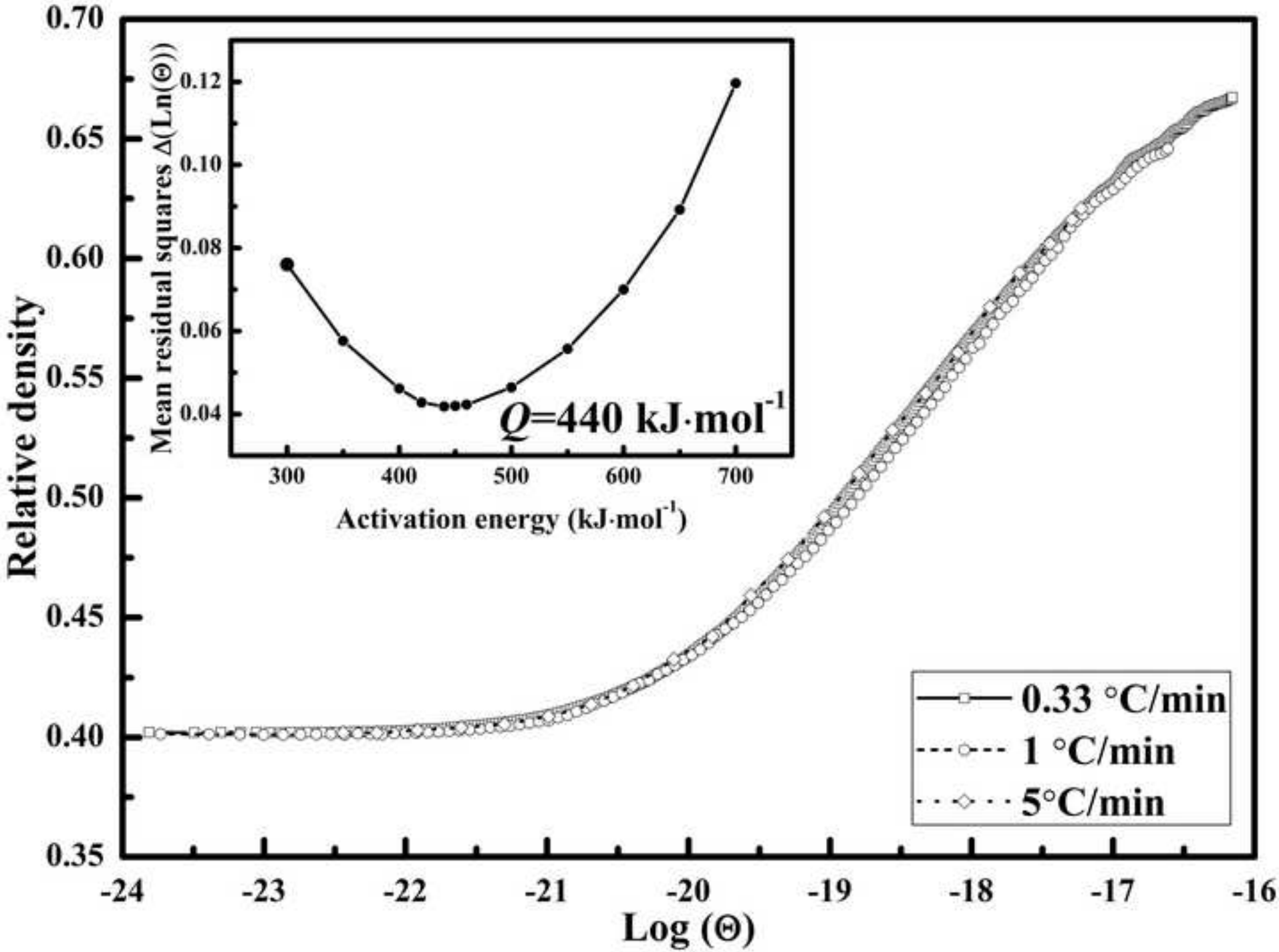

Fig. 5.tif
Click here to download high resolution image

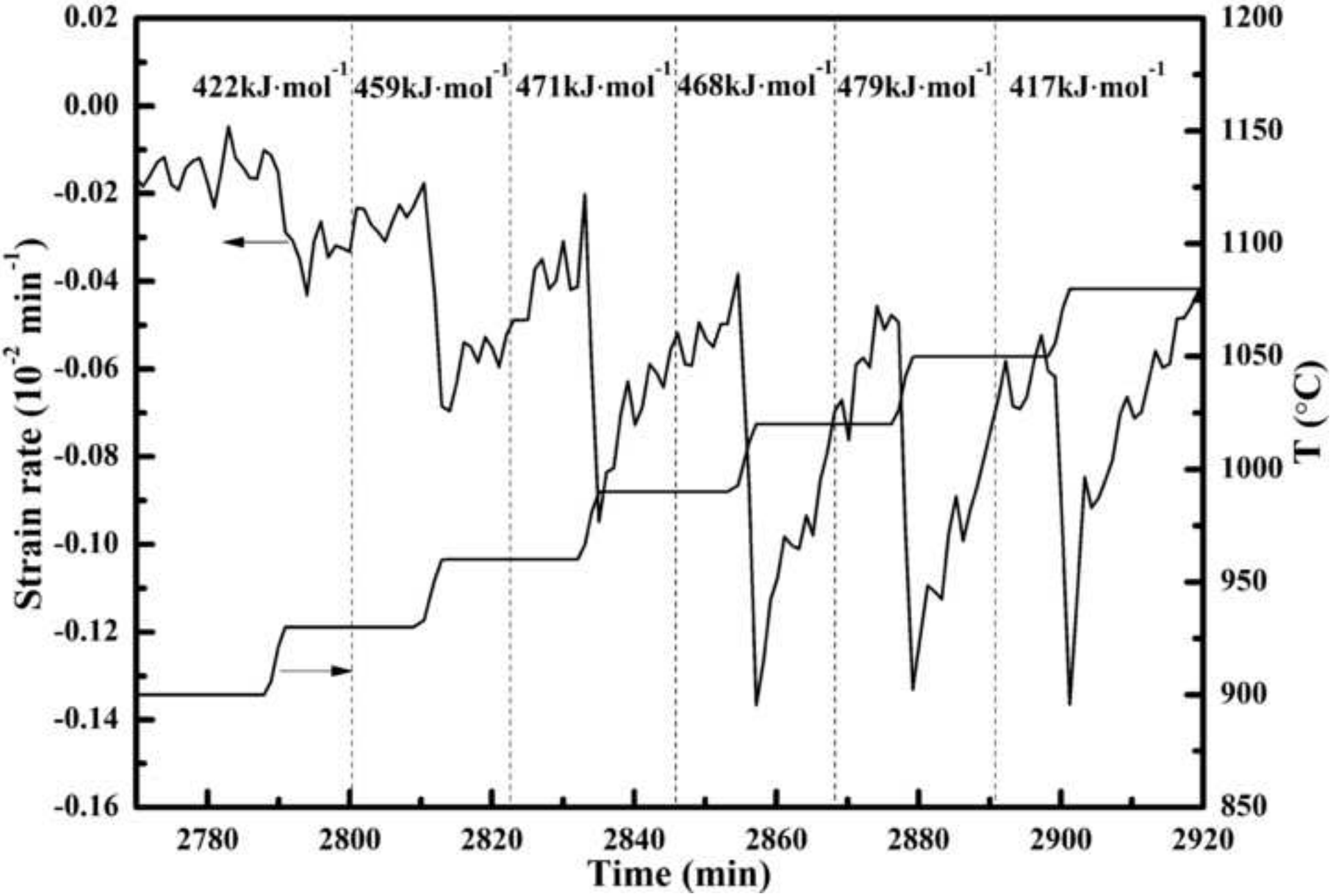

Fig. 6.tif
Click here to download high resolution image

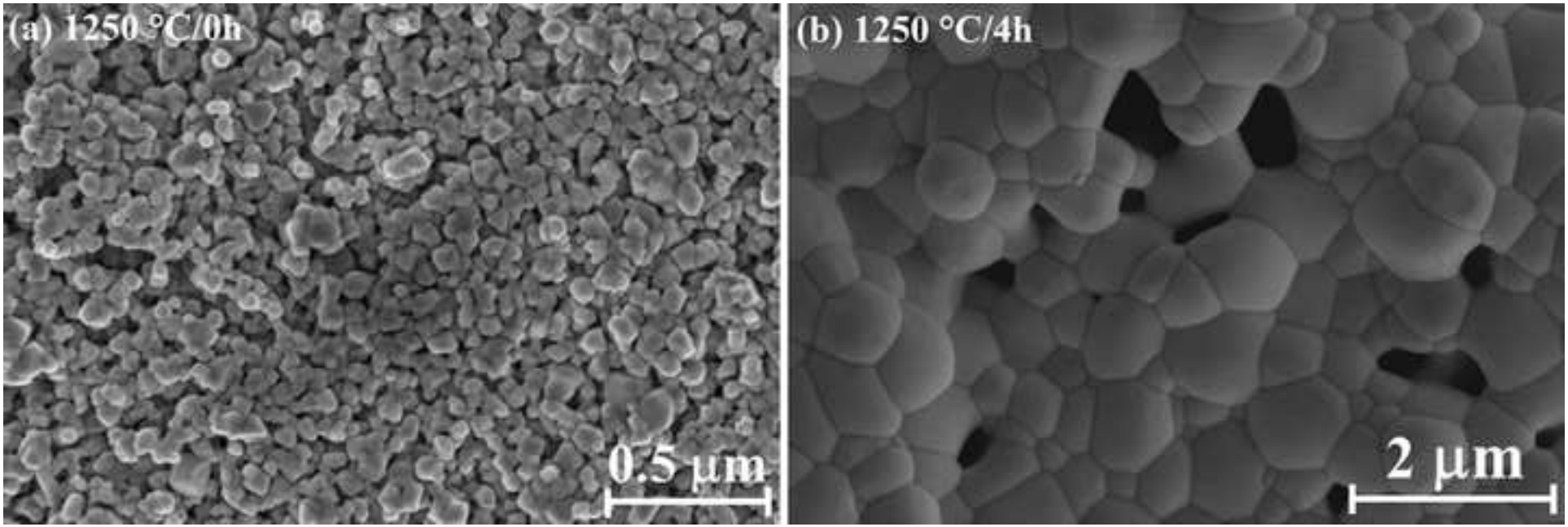

Fig. 7.tif

Click here to download high resolution image

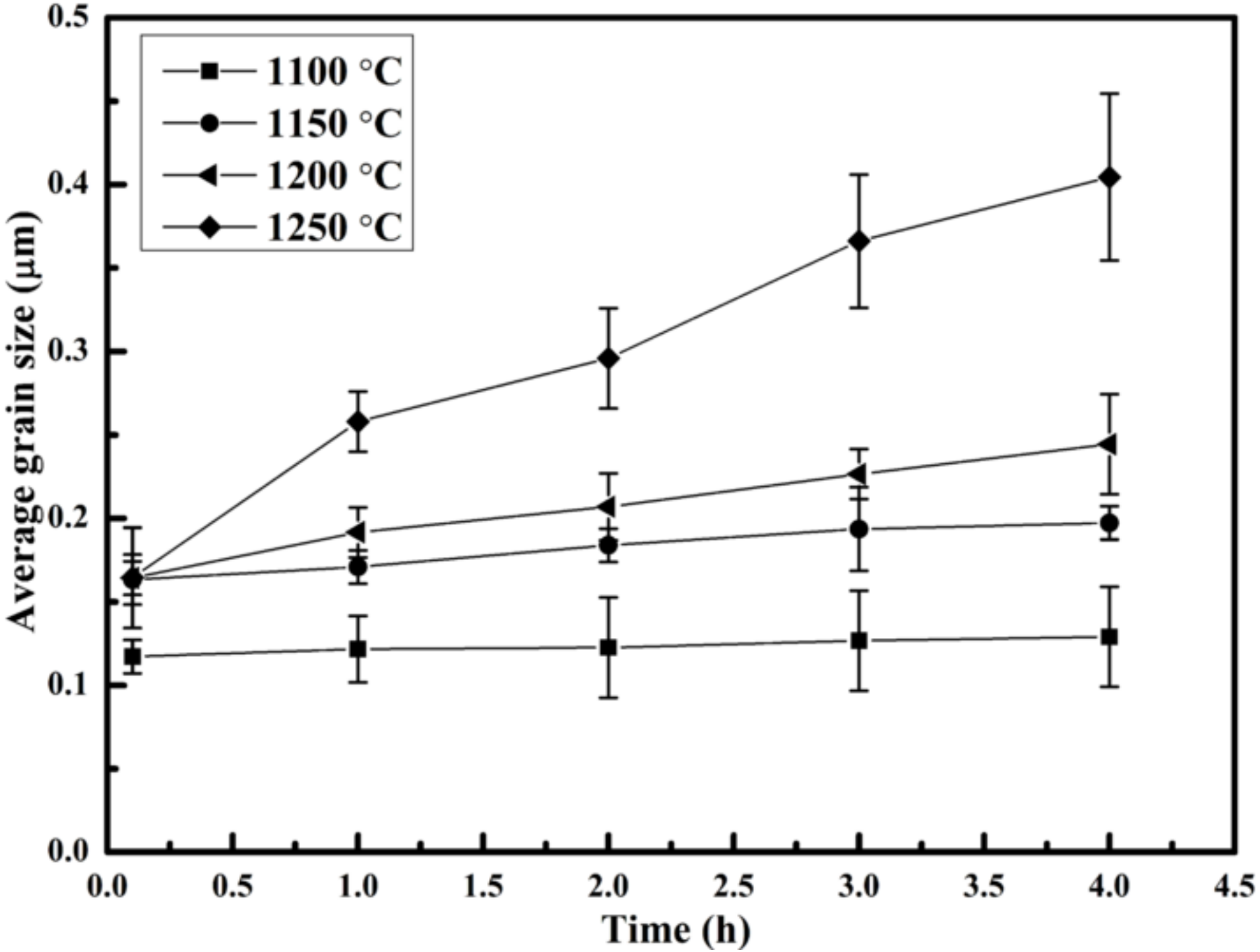

Fig. 8.tif

Click here to download high resolution image

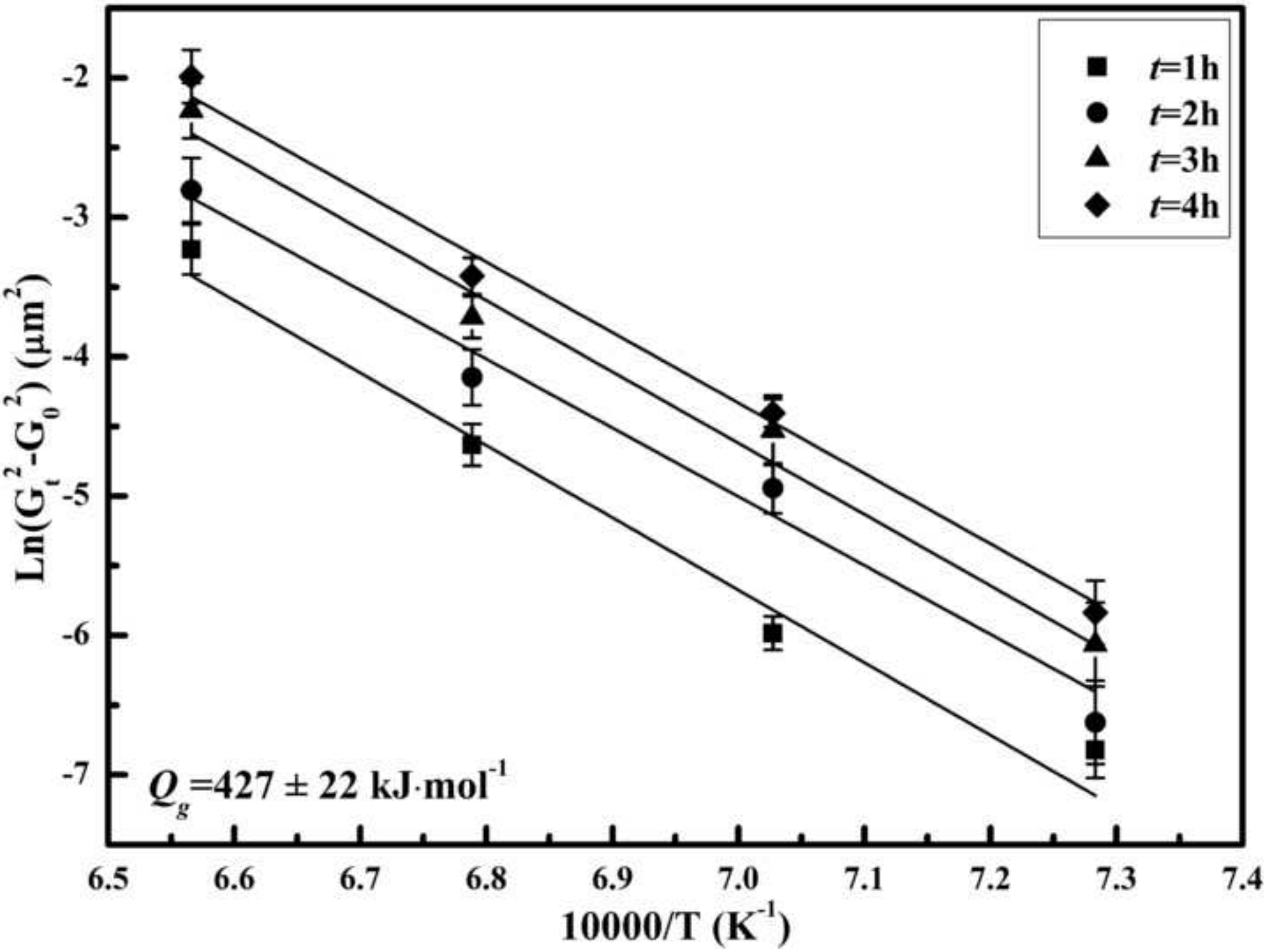

Fig. 9.tif
Click here to download high resolution image